Posted on 9 Feb 2023 — The copyright holder is the author/funder. All rights reserved. No reuse without permission. — https://doi.org/10.22541/essoar.167590830.09227890/v1 — This a preprint and has not been peer reviewed. Data may be preliminary.

Deepening of Southern Ocean gateway leads to abrupt onset of a deep-reaching meridional overturning circulation

Qianjiang Bryant Xing[1], Andreas Klocker[2], David R Munday[3], and Joanne M Whittaker[1]

[1]University of Tasmania
[2]NORCE Norwegian Research Centre
[3]British Antarctic Survey

February 9, 2023

Abstract

During the Eocene-Oligocene transition, the meridional overturning circulation underwent large changes, associated with the geological evolution of Southern Ocean gateways. These are crucial for the Cenozoic climate transition from Greenhouse to Icehouse, but their dynamics still remain elusive. We demonstrate, using an idealised eddying ocean model, that the opening of a gateway leads to an abrupt onset of a vigorous, deep-reaching, meridional overturning circulation. This meridional overturning circulation has a maximum transport for a shallow gateway, and decreases with further deepening of the gateway. This abrupt change in the meridional overturning circulation can be explained through the ability with which standing meanders – turbulent features located downstream of the gateway – can induce deep vertical heat transport at high latitudes where bottom waters are produced. Our results demonstrate the crucial role of turbulent processes, associated with tectonic evolution, in setting the strength of the global ocean's deep-reaching meridional overturning circulation.

Deepening of Southern Ocean gateway leads to abrupt onset of a deep-reaching meridional overturning circulation

Qianjiang Xing[1], Andreas Klocker[2], David Munday[3], Joanne Whittaker[1]

[1]Institute for Marine and Antarctic Studies, University of Tasmania, Hobart, Australia
[2]NORCE Norwegian Research Centre, Bjerknes Centre for Climate Research, Bergen, Norway
[3]British Antarctic Survey, Cambridge, United Kingdom

Key Points:

- The shallow opening of an ocean gateway leads to an abrupt onset of a deep-reaching overturning circulation.
- The deep-reaching overturning circulation is a consequence of standing meanders allowing for full-depth vertical heat transport.
- Further deepening of the gateway leads to a weaker overturning due to a decrease in heat transport towards southern convection regions.

Corresponding author: Qianjiang Xing, `qianjiang.xing@utas.edu.au`

Abstract

During the Eocene-Oligocene transition, the meridional overturning circulation underwent large changes, associated with the geological evolution of Southern Ocean gateways. These are crucial for the Cenozoic climate transition from Greenhouse to Icehouse, but their dynamics still remain elusive. We demonstrate, using an idealised eddying ocean model, that the opening of a gateway leads to an abrupt onset of a vigorous, deep-reaching, meridional overturning circulation. This meridional overturning circulation has a maximum transport for a shallow gateway, and decreases with further deepening of the gateway. This abrupt change in the meridional overturning circulation can be explained through the ability with which standing meanders – turbulent features located downstream of the gateway – can induce deep vertical heat transport at high latitudes where bottom waters are produced. Our results demonstrate the crucial role of turbulent processes, associated with tectonic evolution, in setting the strength of the global ocean's deep-reaching meridional overturning circulation.

Plain Language Summary

Around 50-34 million years ago, the Southern Hemisphere witnessed a major reorganisation of continents. This led to the opening and deepening of two Southern Ocean gateways - the Tasmanian Gateway between Australia and Antarctica, and Drake Passage between Cape Horn and the Antarctica Peninsula. During this period Earth's climate went through a major climate transition, from a hot Greenhouse world to a cold Icehouse world. One hypothesis to explain this dramatic climate transition is that the opening of these ocean gateways led to a major transition in the ocean's overturning circulation (i.e. it's vertical circulation) with important consequences for the ocean's capability to store heat and carbon. In this study we use an ocean model to understand how the opening of an ocean gateway affects the ocean's overturning circulation. We show that it is small-scale processes, and their ability to transport heat southward and downward, which lead to an abrupt onset of the ocean's overturning circulation as soon as the ocean gateway opens. Further deepening of the ocean gateways then leads to a decrease in the overturning circulation. This study therefore highlights the crucial role of small-scale processes in changing Earth's climate.

1 Introduction

The long-term investigation into the meridional overturning circulation (MOC) is primarily motivated by its prominent role in the global redistribution of heat and cycling of chemical elements (Kuhlbrodt et al., 2007; Talley, 2013; Cessi, 2019). In the widely accepted paradigm, the modern MOC is composed of an upper cell, associated with the formation of North Atlantic Deep Water in the Nordic Seas, and a lower overturning cell, associated with the formation of Antarctic Bottom Water around the Antarctic coast (G. C. Johnson, 2008; Marshall & Speer, 2012; H. L. Johnson et al., 2019). The initiation of the modern MOC can be traced to the Eocene-Oligocene transition (EOT, $\sim$34 Ma) (Hohbein et al., 2012; Thomas et al., 2014; Boyle et al., 2017; Ferreira et al., 2018; Hutchinson et al., 2021). Before this time, throughout the Paleocene and early Eocene ($\sim 65{-}40$ Ma), geological evidence points towards a bipolar mode of the MOC in the Pacific basin, with convection occurring both in the North Pacific and the Southern Ocean (Thomas, 2004; Hague et al., 2012; Thomas et al., 2014).

The transition of the Eocene MOC to a modern-like MOC is thought to have occurred around the EOT (Katz et al., 2011; Borrelli et al., 2014; Hutchinson et al., 2021), triggered by tectonic changes. These tectonic changes involved the opening and deepening of the ocean gateways, such as Greenland-Scotland Ridge and Southern Ocean gateways (Katz et al., 2011; Abelson & Erez, 2017; Borrelli et al., 2014; Hutchinson et al., 2021). The deepening of Drake Passage (DP), for example, is thought to have led to deep water upwelling in the Southern Ocean driven by wind stress, closing the modern type MOC (Toggweiler & Bjornsson, 2000; Sijp & England, 2004). While many studies focus on understanding changes in the MOC between fully open and fully closed gateways, recent work has shown how a progressive deepening of the DP affects the global MOC (Toumoulin et al., 2020). Before the opening of the DP, southern sinking occurs in the Atlantic basin and is constrained to shallow depth (Toumoulin et al., 2020). After the opening of the DP to 100 m depth, southern sinking partially shifts to the Pacific, and the global MOC abruptly strengthens to almost twice modern values, but weakens for a further gateway deepening (Toumoulin et al., 2020). These simulations, showing the effect of the progressive deepening of the DP on the MOC, have been run with a complex Earth System model with a coarse-resolution ocean, and hence turbulent processes, such as mesoscale eddies, need to be parameterised. As such, it is difficult to pin down the exact ocean dynamics leading to this radical change in the MOC.

The deepening of ocean gateways forms large local bathymetric features, such as ridges and seamounts. These bathymetric features have profound effects on the dynamics of the Antarctic Circumpolar Current (ACC), generating Rossby waves due to jets in the ACC interacting with these bathymetric features. Rossby waves propagate westward against the ACC mean flow (C. W. Hughes, 2005; Zhang et al., 2023). When their propagation speed matches the speed of the eastward-flowing ACC, these Rossby waves become standing Rossby waves, also known as standing meanders (C. W. Hughes, 2005). Mathematically, standing meanders can be presented as time-mean deviations from the zonal-mean component of the ACC (Ivchenko et al., 1996; Youngs et al., 2017). Standing meanders in the modern ACC influence heat transport and closure of the overturning circulation (Youngs et al., 2017). For example, hot spots of eddy heat flux along the ACC occur around major bathymetric features where standing meanders occur. This indicates that they may contribute to strong poleward heat transport across the ACC (Foppert et al., 2017). However, the role of standing meanders during gateway deepening, such as that during the EOT, is uncertain since coarse-resolution ocean models used in these studies do not resolve these turbulent processes, and it is unclear how well parameterisations of these processes work.

In this work, we use an idealised sector model to understand the role of gateway deepening on the lower overturning cell. The model domain is that of a narrow sector with a blocked ocean basin, such as the Atlantic basin, to the north, and a zonally reentrant channel, such as the Southern Ocean, to the south. Due to the limited size of the domain, it is possible to use a horizontal resolution which allows for the representation of mesoscale eddies, whilst remaining computationally efficient. This allows for the long spinup necessary to achieve statistical equilibrium. This work builds on results of Klocker et al. (submitted), who used the same model configuration, but with only a fully closed and fully open OG, to understand how buoyancy forcing alone can generate a deep-reaching lower overturning cell, similar to that observed. We use this configuration to analyse changes in ocean dynamics when we introduce different gateway depths to the model geometry and seek to answer the following two questions based on Toumoulin et al.'s simulation – why does the initial open of the DP generate a vigorous MOC, and why does the simulated global MOC weaken with the deepening of the DP?

2 Methods

2.1 Model and simulations

The model configuration is based on an ocean-only sector model domain using the MIT general circulation model (MITgcm) (Marshall, Hill, et al., 1997; Marshall, Adcroft, et al., 1997). As shown in Figure 1, the model domain is composed of an ocean basin extending from 60°S to 60°N, and 0°E to 20°E. An ocean gateway is located in the latitudes of 60°S to 40°S. We refer to the ocean gateway as "OG" for the sake of convenience. The model domain has 1/6 ° horizontal grid spacing, allowing for mesoscale eddies. There are 42 unevenly spaced vertical levels with a 10 m thickness at the surface level, stretching to 250 m at the bottom, for a total depth of 5000 m. At the surface, temperature is restored to a fixed distribution, with a restoring time scale of 10 days. The sea surface temperature at the equator is restored to 30°C, the southern end of the domain to 0°C, and the northern end of the domain to 5°C. A linear equation of state is used for density with a constant salinity of 35 psu. There is no wind forcing or other mechanical forcing. The background vertical diffusivity is set to $K_v = 10^{-6}$ m^{2}s^{-1}. More details of the model configuration can be found in Klocker et al.(submitted).

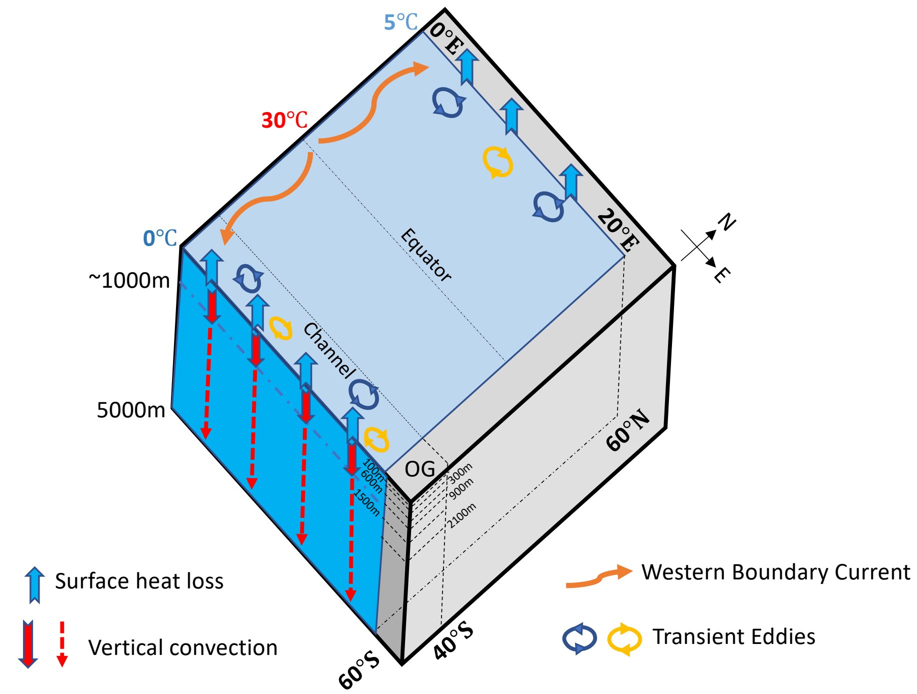

Figure 1. Schematic of model domain and ocean circulation. Orange curved arrows indicate western boundary current. In the channel (60°S - 40°S), colored circles are transient eddies, blue vertical arrows are surface heat loss. Solid (dashed) red vertical arrows at the southern end indicate convection in the cases of *OG_closed* (all experiments with an open OG).

An experiment with both a fully closed OG (*OG_closed*), and a fully open OG (*OG_open*), were run for 3000 model years in Klocker et al.(submitted). Based on these two existing cases, we conduct six sensitivity experiments in which we change the OG depths (the depth of the OG topography beneath sea surface) to 100 m (*OG_100*), 300 m (*OG_300*), 600 m (*OG_600*), 900 m (*OG_900*), 1500 m (*OG_1500*) and 2100 m (*OG_2100*). We run all six sensitivity experiments for 2500 model years from the *OG_closed* case, and use the final 50 years for our analysis.

2.2 Calculation of the meridional overturning circulation

To accurately describe the MOC, composed of horizontal and vertical flows along and across density surfaces, it is necessary to calculate the MOC in density coordinates

(Döös & Webb, 1994). We calculate the meridional transport (VH) between every density layer, where V is meridional velocity and H is thickness of density layer. We take the vertical integral of VH, then zonally integral and finally average over time to get the total MOC in density coordinates (Ballarotta et al., 2013), which can be written as:

$$\Psi^{\sigma}_{total} = \frac{1}{t_1 - t_0} \int_{t_0}^{t_1} \int_{x_W}^{x_E} \sum_{z^s_\sigma(\sigma)}^{z^b_\sigma(\sigma)} VH \, dx \, dt, \tag{1}$$

where x_W and x_E are the longitudes of the western and eastern boundaries of the model domain. z^s_σ and z^b_σ are surface and bottom density layer. t_0 and t_1 are the start and end point of the time average, respectively. Noting that the vertical sum is vertically accumulating density-binned VH.

We then use the thickness of density layers ($z_\sigma(\sigma)$) and the time-average density distribution in depth coordinates ($\sigma(x, y, z)$) to linearly interpolate the density-coordinate MOC into depth coordinates:

$$\Psi^{\sigma}_{total} \longrightarrow \Psi^{z}_{total}. \tag{2}$$

2.3 Calculation of meridional heat transport and vertical heat transport

The zonally integrated meridional heat transport (MHT) is calculated on each depth level as

$$MHT = \frac{\rho_0 C_\rho}{t_1 - t_0} \int_{t_0}^{t_1} \int_{x_W}^{x_E} VT \, dx, \tag{3}$$

where V is zonal velocity, T is potential temperature, ρ_0 is the reference density, and C_ρ is the specific heat capacity. When zonally and vertically integrating the meridional heat transport, we get

$$MHT_Z = \frac{\rho_0 C_\rho}{t_1 - t_0} \int_{t_0}^{t_1} \int_{x_W}^{x_E} \int_{z_b}^{z_s} VT \, dz \, dx \, dt, \tag{4}$$

where z^s and z^b are surface and bottom depth layer.

The vertical heat transport (VHT) is calculated by horizontally integrating the vertical advective flux of potential temperature at each depth level,

$$VHT = \frac{\rho_0 C_\rho}{t_1 - t_0} \int_{t_0}^{t_1} \int_{A} WT \, dA \, dt, \tag{5}$$

where W is the vertical velocity and A is horizontal area of the ocean domain.

2.4 Decomposition into eddy, standing-meander, and mean components

Using Reynolds averaging, an arbitrary field B can be decomposed into its time mean, $\overline{B}$, and transient eddy, B', components:

$$B = \overline{B} + B'. \tag{6}$$

Note that, by construction, $\overline{B'} = 0$.

The time mean component, $\overline{B}$, can be further separated into its zonal average part $\langle\overline{B}\rangle$ and the excursion from this average $\overline{B^*}$ (the so-called standing meanders component):

$$\overline{B} = \langle\overline{B}\rangle + \overline{B^*}. \tag{7}$$

The total field, B, is then given by:

$$B = \langle\overline{B}\rangle + \overline{B^*} + B'. \tag{8}$$

We can use Reynolds averaging to decompose the total transport of any tracer, such as temperature, into its mean, eddy, and standing meander components. The times and zonal averages operate on the product of meridional velocity and temperature in the equation (3). This produces three terms, since the covariance of $V^{'}$ and $T^{'}$ is not zero by construction. We can then decompose the total MHT_Z into three components:

$$MHT_Z = \rho_0 C_\rho \int_{x_W}^{x_E} \int_{z_b}^{z_s} \left[\langle \overline{V} \rangle \, \langle \overline{T} \rangle + \overline{V^* T^*} + \overline{V' T'} \right] \, dz \, dx, \tag{9}$$

where the first term of right side is mean flow component ($\langle \overline{MHT} \rangle_Z$), the second term is the standing meander component (MHT^*_Z), and the third term is transient eddy component ($MHT^{'}_Z$). Similarly, we use this decomposition for the vertical heat transport, giving $\langle \overline{VHT} \rangle$, VHT^* and $VHT^{'}$.

3 Results

3.1 Overturning circulation with fully open and fully closed gateway

Due to the heating of the ocean surface at the equator and cooling at high latitudes, ocean circulation adjusts to allow for a heat transport from the equator to high latitudes through a process known as (rotating) horizontal convection (G. O. Hughes & Griffiths, 2008; Gayen & Griffiths, 2022). In a closed basin, such as in experiment *OG_closed*, meridional boundaries allow for the generation of an east-west pressure gradient, and hence the poleward heat transport is due to western boundary currents (WBCs) associated with ocean gyres (Figure S1b). These WBCs transport heat poleward very efficiently and lead to a shallow MOC (Figure 2a), consistent with previous results (Klocker et al., submitted).

In the absence of meridional boundaries, such as in experiment *OG_open*, WBCs cannot exist in the latitude range of the channel (Figure S1j). At these latitudes only turbulent processes, such as mesoscale eddies, can transport heat across the channel (Figure 4i,j). These mesoscale eddies are generated by baroclinic instability due to steeply sloping density surfaces across the channel. These surfaces also generate a circumpolar current, resembling the Antarctic Circumpolar Current (Figure S1i), via thermal wind balance. As shown by Klocker et al. (submitted), the presence of eddies allows for a deep-reaching MOC, as opposed to the shallow MOC observed in the presence of meridional boundaries. In experiment *OG_open*, the surface buoyancy forcing generates a lower overturning cell with a strength (T_{MOC}) of 0.89 Sv, which is equivalent to 16.02 Sv when extrapolated from the width of the sector model to the full width of the ocean (Figure 2h,i).

For both *OG_closed* and *OG_open*, the MOC is closed by vertical plumes against the northern and southern headwall of the domain (G. Hughes et al., 2007; Gayen & Griffiths, 2022). In these regions, a destabilising buoyancy flux at the ocean surface leads to the formation of deep and bottom waters (Gayen & Griffiths, 2022). The heat in both cases can be transported by mean flows in the form of western boundary currents, or by mesoscale eddies across the re-entrant channel to generate an overturning cell. Below we will show that in the cases of partially open gateway there is a third process – standing meanders – which can lead to lateral and vertical heat transport, allowing for the formation of a deep-reaching MOC.

3.2 Deep-reaching overturning circulation with gateway deepening

A shallow OG, as in experiment *OG_100*, allows the formation of a vertically-sheared circumpolar current (Figure 2i). This circumpolar current is the result of the combination of buoyancy loss at the southern boundary, which, together with the lack of meridional boundaries above the OG depth, leads to the steepening of density surfaces and hence a (weak) associated circumpolar current with a zonal transport (T_{ACC}) of 3.1 Sv

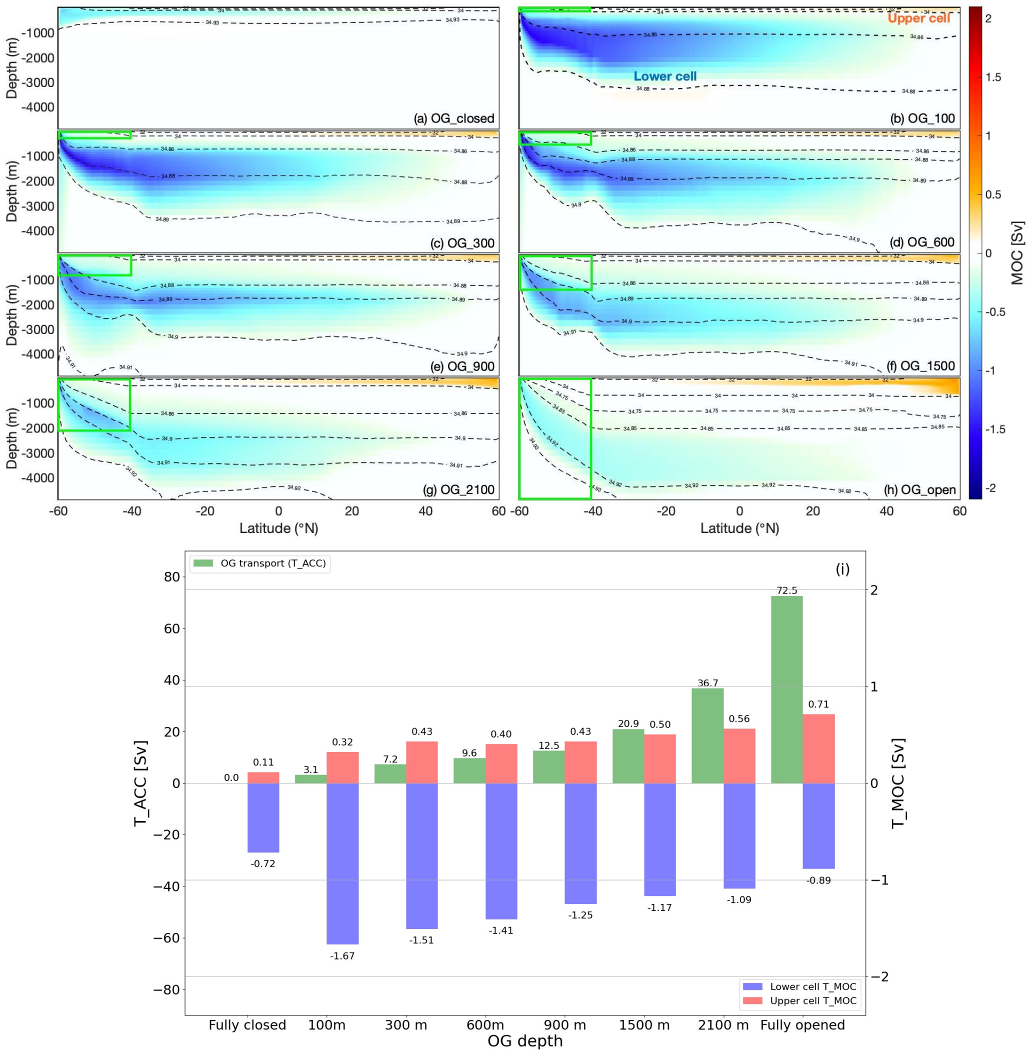

Figure 2. (a)-(h) MOC [Sv] of all simulations; clockwise cell (red) is the upper overturning cell and counterclockwise cell (blue) is the lower overturning cell. (i) Transport through OG ($T_{ACC}[Sv]$; green), maximum MOC ($T_{MOC}[Sv]$) for the upper cell (red) and the lower cell (blue).

(Figure 2i). This circumpolar current is baroclinically unstable, resulting in the generation of transient eddies and standing meanders, with the latter being generated due to the circumpolar current interacting with the topography of the OG.

A striking change is the deep-reaching MOC in *OG_100*; despite the very shallow OG, the lower overturning cell now extends to about 3500 m, and increases from 0.72 Sv in *OG_closed* to 1.67 Sv (global scale: 30.06 Sv; Figure 2b,i). This formation of a strong deep-reaching lower overturning cell is consistent with results by Klocker et al. (submitted), who showed how mesoscale eddies allow for a full-depth overturning cell, and with results by Toumoulin et al. (2020) who used a coarse-resolution earth system model with a 100 m deep DP and Eocene boundary conditions to simulate changes in the MOC due to gateway deepening.

With the deepening of the OG from 100 m to 2100 m (experiments *OG_100* to *OG_2100*), the transport of the eastward circumpolar current (T_{ACC}) gradually increases to 36.7 Sv (Figure 2i). In contrast with the increasing transport of the circumpolar current, the lower overturning cell continuously weakens to 1.09 Sv (global scale: 19.62 Sv) for the 2100 m OG experiment (Figure 2i). The shallowest OG therefore leads to the strongest lower overturning cell. This is consistent with recent results using a complex earth system model (Toumoulin et al., 2020).

3.3 The role of ocean heat transport

Buoyancy (heat) loss at the southern boundary of the channel leads to deep convection (Gayen & Griffiths, 2022) and hence the lower overturning cell. In an equilibrated ocean, maintaining the buoyancy loss and a deep-reaching overturning requires continuous lateral heat transport towards the southern ('Antarctic') boundary, and vertical heat transport to the deep ocean. The lower overturning cell is accordingly controlled by this heat transport. In this section, we will show how changes in OG depth affect the distribution of meridional and vertical heat transport by mean flows, standing meanders, and transient eddies.

For the experiment with a closed OG (*OG_closed*), the zonally integrated meridional heat transport is dominated by the mean flow (Figure 3a,b), transporting heat southward (blue colours) at the surface and northward (red colours) below. This is consistent with the MOC being confined to the shallow ocean, with the deep ocean being largely at rest (Figure 2a and Figure 3a-c). In the southern hemisphere, standing meanders produce a southward MHT (MHT^*) at the surface, and a northward MHT below. Transient eddies lead to a southward MHT across the channel, but contribute less to the heat transport than either the mean flow or standing meanders (Figure S4). The vertically integrated MHT (MHT_Z) is strongly biased towards the southern high latitudes, consistent with experiments of thermally-driven flows in a domain lacking a re-entrant channel, in which the flow is biased towards the pole with the colder temperature forcing (Coman et al., 2010, Figure 4a). Consistent with the shallow confinement of the MHT and MOC, the VHT is confined to the shallow ocean (Figure 4b). In summary, in *OG_closed* the entire heat transport is by baroclinic gyres which are confined to the ocean surface, leading to a shallow MOC. The deep ocean is at rest.

When the OG opens to a depth of 100 m (*OG_100*), the MHT suddenly extends to the full depth of the basin rather than being confined to the shallow ocean, with a southward MHT from surface to mid-depth, and a northward MHT below (Figure 3e). This corresponds to a full-depth lower overturning cell, which increases in strength from 0.72Sv to 1.67Sv. Standing meanders lead to a southward MHT above the OG depth, and a northward MHT below the OG depth (Figure 3f). Transient eddies still provide weak southward MHT in the channel. The total vertically and zonally integrated southward MHT (${MHT^*}_Z$) in the southern half of the basin is reduced by about half (maximum about -10 TW) compared to *OG_closed*, and is both due to the mean flow and standing me-

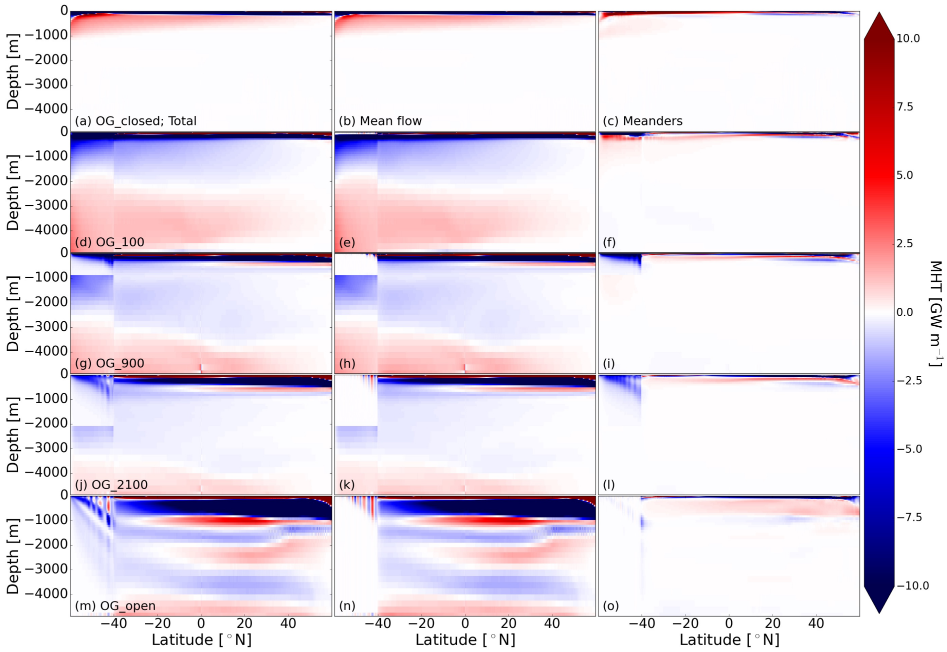

Figure 3. Hydrographic section of the zonally integrated meridional heat transport (MHT) [GW m^{-1}] for experiments *OG_closed*, *OG_100*, *OG_900*, *OG_2100*, and *OG_open*. Left panels show total MHT, middle panels show the MHT by the mean flow ($\langle\overline{MHT}\rangle$), and right panels show the MHT by standing meanders (MHT^{*}).

anders (Figure 4c). On the other hand, the northward MHT in the northern half of the basin increases by 8 TW compared to *OG_closed*. Transient eddies again provide little MHT (MHT'_{Z}) relative to the mean flow and standing meanders. In contrast to the large decrease in MHT by the mean flow in *OG_100*, the VHT by the mean flow shows a large increase in strength and now extends to the full depth (Figure 4d).

For a further OG deepening (from *OG_100* to *OG_2100*), the mean MHT in the deep ocean decreases in strength compared with *OG_100*, reflected by lighter blue and red colors in the Figure 3h and k. This corresponds to a weakening of the deep-reaching MOC. In the channel, standing meanders lead to a southward MHT above the OG depth. The MHT by transient eddies increases, although it is still weaker than the other terms. The gradual deepening of the OG strengthens the transport of the circumpolar current, and leads to a state where the vertically integrated MHT is entirely due to standing meanders (Figure 4e and g) in the channel. The MHT by standing meanders becomes weaker the deeper the OG, leading to a decrease in strength of the lower overturning cell for a further OG deepening. This weakening of the southward MHT is accompanied by a strengthening of the northward MHT, and hence a stronger upper overturning cell.

When the OG is fully open (*OG_open*), standing meanders cannot exist since their existence relies on the interaction with a ridge, and instead transient eddies provide southward MHT. For this experiment the MOC is still full-depth, but weaker than in all cases where standing meanders are present. This experiment therefore shows that eddies are also capable of allowing for a full-depth lower overturning cell, but given that transient eddies are less efficient at transporting heat towards the southern convection region, the lower overturning cell is weaker than in all cases where standing meanders are present.

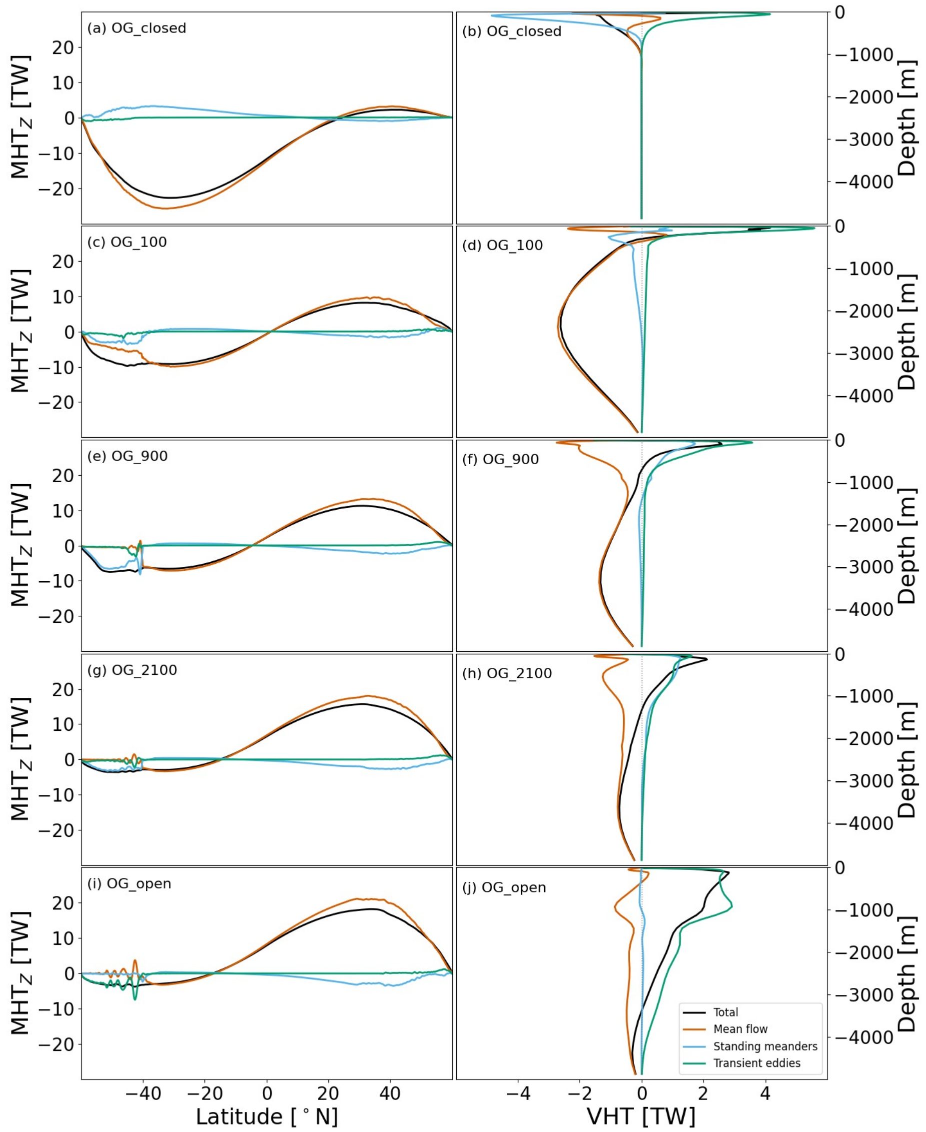

Figure 4. (a,c,e,g,i) Zonally and vertically integrated meridional heat transport (MHT_Z) [TW] for experiments *OG_closed*, *OG_100*, *OG_900* , *OG_2100*, and *OG_open*. (b,d,f,h,j) Horizontal integrated vertical heat transport (VHT) [TW] in the channel for experiments *OG_closed*, *OG_100*, *OG_900*, *OG_2100*, and *OG_open*. In all panels, black lines indicate the total (MHT_Z/VHT), red lines the mean component ($\langle\overline{MHT}\rangle_Z/\langle\overline{VHT}\rangle$), green lines the standing meanders ($MHT^*{}_Z/VHT^*$), and blue lines the transient eddies ($MHT^{'}{}_Z/VHT^{'}$).

4 Discussion and Conclusion

In summary, the evolution of the deep-reaching lower overturning cell with the deepening of the ocean gateway can be divided into two parts: the abrupt onset of the deep-reaching lower overturning cell for a shallow ocean gateway, and the subsequent weakening for a further deepening of the ocean gateway. This behaviour of the lower overturning cell is closely linked to changes in southward and downward heat transport in the presence of standing meanders. First, in an equilibrated ocean, the strength of an overturning cell is limited by the amount of heat which can be supplied to the vertical plumes associated with strong surface buoyancy loss. This heat supply is most efficient if mean flows, such as western boundary currents, are present. This heat supply becomes less efficient if the heat transport is due to standing meanders, and even less efficient if heat supply is due to transient eddies. A deepening ocean gateway therefore leads to a reduced southward heat transport, which is compensated with an increase in northward heat transport. Second, a deep-reaching overturning cell is dependent on a process which can get this heat to depth. As shown by Klocker et al. (submitted), this can be achieved by transient eddies, and, as shown here, this can also be achieved by standing meanders. Nevertheless, heat transport by baroclinic gyres is always confined to the surface, and the presence of mesoscale turbulence, whether transient eddies or standing meanders, is necessary to get this heat to depth, and hence lead to a deep-reaching MOC.

The two-part evolution of the lower overturning cell for a deepening of an ocean gateway is therefore a combination of the two roles transient eddies and standing meanders play for ocean heat transport. These dynamics lead to a maximum lower overturning cell for the experiment with the shallowest OG, which is a combination of the domain where the southward heat transport is largest, while at the same time allowing for a deep-reaching heat transport by mesoscale turbulence. Further deepening of the OG leads to a weakening of the southward heat supply across the channel, and a strengthening of the northward heat transport, associated with a strengthening of the upper overturning cell. Once the OG is as deep as the rest of the domain, the southward heat transport is solely due to transient eddies, resulting in the weakest deep-reaching overturning cell. As opposed to studies which focus on just fully open and fully closed OGs, we highlight the importance of the dynamics of standing meanders in understanding the evolution of the MOC with gateway deepening, a turbulent process generally neglected in the paleoceanography community.

Previous studies have used complex, but coarse-resolution, earth system models to explain the evolution of the global MOC with the deepening of Southern Ocean gateways (Sijp & England, 2004; Toumoulin et al., 2020). However, in these studies results contradict each other, with (Sijp & England, 2004) showing the strongest MOC for a closed OG, while (Toumoulin et al., 2020), consistent with our study, showing the strongest MOC for a shallow OG. Nevertheless, both these studies show a weakening of the southward meridional heat transport with a deepening of the OG, and a strengthening of the northward meridional heat transport, consistent with our study. The different results for the lower overturning cell are possibly the consequence of the parameterisation of mesoscale turbulence in these models. It is the simple but high-resolution model configuration used in this study that helps to reveal the critical role of turbulence processes in generating the strong deep-reaching overturning cell with OG deepening. Future work is planned to extend this work on the evolution of the EOT MOC with a global ocean model and realistic paleo-bathymetry.

5 Data Availability Statement

All model output used in this study to perform the analysis and produce figures is available at https://doi.org/10.5281/zenodo.7602996.

Acknowledgments

This work was supported by the Australian Research Council Discovery Project (DP180102280). QX was supported by scholarships from the Australian Government Research Training Program (RTP) and CSIRO-UTAS PhD Program in Quantitative Marine Science (QMS). We acknowledge the Australian National Computational Infrastructure Merit Allocation Scheme projects and Australian Antarctic Division grant AAS4567 for running the model simulations.

References

Abelson, M., & Erez, J. (2017). The onset of modern-like a tlantic meridional overturning circulation at the e ocene-o ligocene transition: Evidence, causes, and possible implications for global cooling. *Geochemistry, Geophysics, Geosystems*, *18*(6), 2177–2199.

Ballarotta, M., Drijfhout, S., Kuhlbrodt, T., & Döös, K. (2013). The residual circulation of the southern ocean: Which spatio-temporal scales are needed? *Ocean Modelling*, *64*, 46–55.

Borrelli, C., Cramer, B. S., & Katz, M. E. (2014). Bipolar atlantic deepwater circulation in the middle-late eocene: Effects of southern ocean gateway openings. *Paleoceanography*, *29*(4), 308–327.

Boyle, P. R., Romans, B. W., Tucholke, B. E., Norris, R. D., Swift, S. A., & Sexton, P. F. (2017). Cenozoic north atlantic deep circulation history recorded in contourite drifts, offshore newfoundland, canada. *Marine Geology*, *385*, 185–203.

Cessi, P. (2019). The global overturning circulation. *Annual review of marine science*, *11*, 249–270.

Coman, M., Griffiths, R., & Hughes, G. (2010). The sensitivity of convection from a horizontal boundary to the distribution of heating. *Journal of Fluid Mechanics*, *647*, 71–90.

Döös, K., & Webb, D. J. (1994). The deacon cell and the other meridional cells of the southern ocean. *Journal of Physical Oceanography*, *24*(2), 429–442.

Ferreira, D., Cessi, P., Coxall, H. K., De Boer, A., Dijkstra, H. A., Drijfhout, S. S., ... others (2018). Atlantic-pacific asymmetry in deep water formation. *Annual Review of Earth and Planetary Sciences*, *46*, 327–352.

Foppert, A., Donohue, K. A., Watts, D. R., & Tracey, K. L. (2017). Eddy heat flux across the a ntarctic c ircumpolar c urrent estimated from sea surface height standard deviation. *Journal of Geophysical Research: Oceans*, *122*(8), 6947–6964.

Gayen, B., & Griffiths, R. W. (2022). Rotating horizontal convection. *Annual Review of Fluid Mechanics*, *54*, 105–132.

Hague, A. M., Thomas, D. J., Huber, M., Korty, R., Woodard, S. C., & Jones, L. B. (2012). Convection of north pacific deep water during the early cenozoic. *Geology*, *40*(6), 527–530.

Hohbein, M. W., Sexton, P. F., & Cartwright, J. A. (2012). Onset of north atlantic deep water production coincident with inception of the cenozoic global cooling trend. *Geology*, *40*(3), 255–258.

Hughes, C. W. (2005). Nonlinear vorticity balance of the antarctic circumpolar current. *Journal of Geophysical Research: Oceans*, *110*(C11).

Hughes, G., Griffiths, R., Mullarney, J., & Peterson, W. H. (2007). A theoretical model for horizontal convection at high rayleigh number. *Journal of Fluid Mechanics*, *581*, 251–276.

Hughes, G. O., & Griffiths, R. W. (2008). Horizontal convection. *Annu. Rev. Fluid Mech.*, *40*, 185–208.

Hutchinson, D. K., Coxall, H. K., Lunt, D. J., Steinthorsdottir, M., De Boer, A. M., Baatsen, M., ... others (2021). The eocene–oligocene transition: a review of marine and terrestrial proxy data, models and model–data comparisons. *Climate of the Past*, *17*(1), 269–315.

Ivchenko, V. O., Richards, K. J., & Stevens, D. P. (1996). The dynamics of the antarctic circumpolar current. *Journal of physical oceanography*, *26*(5), 753–774.

Johnson, G. C. (2008). Quantifying antarctic bottom water and north atlantic deep water volumes. *Journal of Geophysical Research: Oceans*, *113*(C5).

Johnson, H. L., Cessi, P., Marshall, D. P., Schloesser, F., & Spall, M. A. (2019). Recent contributions of theory to our understanding of the atlantic meridional overturning circulation. *Journal of Geophysical Research: Oceans*, *124*(8), 5376–5399.

Katz, M. E., Cramer, B. S., Toggweiler, J., Esmay, G., Liu, C., Miller, K. G., ... Wright, J. D. (2011). Impact of antarctic circumpolar current development on late paleogene ocean structure. *Science*, *332*(6033), 1076–1079.

Klocker, A., Munday, D., Gayen, B., Roquet, F., & LaCasce, J. H. (submitted). Deep-reaching global ocean overturning circulation generated by surface buoyancy forcing. *Journal of Physical Oceanography*.

Kuhlbrodt, T., Griesel, A., Montoya, M., Levermann, A., Hofmann, M., & Rahmstorf, S. (2007). On the driving processes of the atlantic meridional overturning circulation [Journal Article]. *Reviews of Geophysics*, *45*(2).

Marshall, J., Adcroft, A., Hill, C., Perelman, L., & Heisey, C. (1997). A finite-volume, incompressible navier stokes model for studies of the ocean on parallel computers. *Journal of Geophysical Research: Oceans*, *102*(C3), 5753–5766.

Marshall, J., Hill, C., Perelman, L., & Adcroft, A. (1997). Hydrostatic, quasi-hydrostatic, and nonhydrostatic ocean modeling. *Journal of Geophysical Research: Oceans*, *102*(C3), 5733–5752.

Marshall, J., & Speer, K. (2012). Closure of the meridional overturning circulation through southern ocean upwelling. *Nature Geoscience*, *5*(3), 171–180.

Sijp, W. P., & England, M. H. (2004). Effect of the drake passage throughflow on global climate. *Journal of Physical Oceanography*, *34*(5), 1254–1266.

Talley, L. D. (2013). Closure of the global overturning circulation through the indian, pacific, and southern oceans: Schematics and transports. *Oceanography*, *26*(1), 80–97.

Thomas, D. J. (2004). Evidence for deep-water production in the north pacific ocean during the early cenozoic warm interval. *Nature*, *430*(6995), 65–68.

Thomas, D. J., Korty, R., Huber, M., Schubert, J. A., & Haines, B. (2014). Nd isotopic structure of the pacific ocean 70–30 ma and numerical evidence for vigorous ocean circulation and ocean heat transport in a greenhouse world. *Paleoceanography*, *29*(5), 454–469.

Toggweiler, J., & Bjornsson, H. (2000). Drake passage and palaeoclimate. *Journal of Quaternary Science: Published for the Quaternary Research Association*, *15*(4), 319–328.

Toumoulin, A., Donnadieu, Y., Ladant, J.-B., Batenburg, S., Poblete, F., & Dupont-Nivet, G. (2020). Quantifying the effect of the drake passage opening on the eocene ocean. *Paleoceanography and Paleoclimatology*, *35*(8), e2020PA003889.

Youngs, M. K., Thompson, A. F., Lazar, A., & Richards, K. J. (2017). Acc meanders, energy transfer, and mixed barotropic–baroclinic instability. *Journal of Physical Oceanography*, *47*(6), 1291–1305.

Zhang, X., Nikurashin, M., Peña-Molino, B., Rintoul, S. R., & Doddridge, E. (2023). A theory of standing meanders of the antarctic circumpolar current and their response to wind. *Journal of Physical Oceanography*, *53*(1), 235 - 251. doi: 10.1175/JPO-D-22-0086.1

Deepening of Southern Ocean gateway leads to abrupt onset of a deep-reaching meridional overturning circulation

Qianjiang Xing[1], Andreas Klocker[2], David Munday[3], Joanne Whittaker[1]

[1]Institute for Marine and Antarctic Studies, University of Tasmania, Hobart, Australia
[2]NORCE Norwegian Research Centre, Bjerknes Centre for Climate Research, Bergen, Norway
[3]British Antarctic Survey, Cambridge, United Kingdom

Key Points:

- The shallow opening of an ocean gateway leads to an abrupt onset of a deep-reaching overturning circulation.
- The deep-reaching overturning circulation is a consequence of standing meanders allowing for full-depth vertical heat transport.
- Further deepening of the gateway leads to a weaker overturning due to a decrease in heat transport towards southern convection regions.

Corresponding author: Qianjiang Xing, `qianjiang.xing@utas.edu.au`

Abstract

During the Eocene-Oligocene transition, the meridional overturning circulation underwent large changes, associated with the geological evolution of Southern Ocean gateways. These are crucial for the Cenozoic climate transition from Greenhouse to Icehouse, but their dynamics still remain elusive. We demonstrate, using an idealised eddying ocean model, that the opening of a gateway leads to an abrupt onset of a vigorous, deep-reaching, meridional overturning circulation. This meridional overturning circulation has a maximum transport for a shallow gateway, and decreases with further deepening of the gateway. This abrupt change in the meridional overturning circulation can be explained through the ability with which standing meanders – turbulent features located downstream of the gateway – can induce deep vertical heat transport at high latitudes where bottom waters are produced. Our results demonstrate the crucial role of turbulent processes, associated with tectonic evolution, in setting the strength of the global ocean's deep-reaching meridional overturning circulation.

Plain Language Summary

Around 50-34 million years ago, the Southern Hemisphere witnessed a major reorganisation of continents. This led to the opening and deepening of two Southern Ocean gateways - the Tasmanian Gateway between Australia and Antarctica, and Drake Passage between Cape Horn and the Antarctica Peninsula. During this period Earth's climate went through a major climate transition, from a hot Greenhouse world to a cold Icehouse world. One hypothesis to explain this dramatic climate transition is that the opening of these ocean gateways led to a major transition in the ocean's overturning circulation (i.e. it's vertical circulation) with important consequences for the ocean's capability to store heat and carbon. In this study we use an ocean model to understand how the opening of an ocean gateway affects the ocean's overturning circulation. We show that it is small-scale processes, and their ability to transport heat southward and downward, which lead to an abrupt onset of the ocean's overturning circulation as soon as the ocean gateway opens. Further deepening of the ocean gateways then leads to a decrease in the overturning circulation. This study therefore highlights the crucial role of small-scale processes in changing Earth's climate.

1 Introduction

The long-term investigation into the meridional overturning circulation (MOC) is primarily motivated by its prominent role in the global redistribution of heat and cycling of chemical elements (Kuhlbrodt et al., 2007; Talley, 2013; Cessi, 2019). In the widely accepted paradigm, the modern MOC is composed of an upper cell, associated with the formation of North Atlantic Deep Water in the Nordic Seas, and a lower overturning cell, associated with the formation of Antarctic Bottom Water around the Antarctic coast (G. C. Johnson, 2008; Marshall & Speer, 2012; H. L. Johnson et al., 2019). The initiation of the modern MOC can be traced to the Eocene-Oligocene transition (EOT, $\sim$34 Ma) (Hohbein et al., 2012; Thomas et al., 2014; Boyle et al., 2017; Ferreira et al., 2018; Hutchinson et al., 2021). Before this time, throughout the Paleocene and early Eocene ($\sim 65-40$ Ma), geological evidence points towards a bipolar mode of the MOC in the Pacific basin, with convection occurring both in the North Pacific and the Southern Ocean (Thomas, 2004; Hague et al., 2012; Thomas et al., 2014).

The transition of the Eocene MOC to a modern-like MOC is thought to have occurred around the EOT (Katz et al., 2011; Borrelli et al., 2014; Hutchinson et al., 2021), triggered by tectonic changes. These tectonic changes involved the opening and deepening of the ocean gateways, such as Greenland-Scotland Ridge and Southern Ocean gateways (Katz et al., 2011; Abelson & Erez, 2017; Borrelli et al., 2014; Hutchinson et al., 2021). The deepening of Drake Passage (DP), for example, is thought to have led to deep water upwelling in the Southern Ocean driven by wind stress, closing the modern type MOC (Toggweiler & Bjornsson, 2000; Sijp & England, 2004). While many studies focus on understanding changes in the MOC between fully open and fully closed gateways, recent work has shown how a progressive deepening of the DP affects the global MOC (Toumoulin et al., 2020). Before the opening of the DP, southern sinking occurs in the Atlantic basin and is constrained to shallow depth (Toumoulin et al., 2020). After the opening of the DP to 100 m depth, southern sinking partially shifts to the Pacific, and the global MOC abruptly strengthens to almost twice modern values, but weakens for a further gateway deepening (Toumoulin et al., 2020). These simulations, showing the effect of the progressive deepening of the DP on the MOC, have been run with a complex Earth System model with a coarse-resolution ocean, and hence turbulent processes, such as mesoscale eddies, need to be parameterised. As such, it is difficult to pin down the exact ocean dynamics leading to this radical change in the MOC.

The deepening of ocean gateways forms large local bathymetric features, such as ridges and seamounts. These bathymetric features have profound effects on the dynamics of the Antarctic Circumpolar Current (ACC), generating Rossby waves due to jets in the ACC interacting with these bathymetric features. Rossby waves propagate westward against the ACC mean flow (C. W. Hughes, 2005; Zhang et al., 2023). When their propagation speed matches the speed of the eastward-flowing ACC, these Rossby waves become standing Rossby waves, also known as standing meanders (C. W. Hughes, 2005). Mathematically, standing meanders can be presented as time-mean deviations from the zonal-mean component of the ACC (Ivchenko et al., 1996; Youngs et al., 2017). Standing meanders in the modern ACC influence heat transport and closure of the overturning circulation (Youngs et al., 2017). For example, hot spots of eddy heat flux along the ACC occur around major bathymetric features where standing meanders occur. This indicates that they may contribute to strong poleward heat transport across the ACC (Foppert et al., 2017). However, the role of standing meanders during gateway deepening, such as that during the EOT, is uncertain since coarse-resolution ocean models used in these studies do not resolve these turbulent processes, and it is unclear how well parameterisations of these processes work.

In this work, we use an idealised sector model to understand the role of gateway deepening on the lower overturning cell. The model domain is that of a narrow sector with a blocked ocean basin, such as the Atlantic basin, to the north, and a zonally reentrant channel, such as the Southern Ocean, to the south. Due to the limited size of the domain, it is possible to use a horizontal resolution which allows for the representation of mesoscale eddies, whilst remaining computationally efficient. This allows for the long spinup necessary to achieve statistical equilibrium. This work builds on results of Klocker et al. (submitted), who used the same model configuration, but with only a fully closed and fully open OG, to understand how buoyancy forcing alone can generate a deep-reaching lower overturning cell, similar to that observed. We use this configuration to analyse changes in ocean dynamics when we introduce different gateway depths to the model geometry and seek to answer the following two questions based on Toumoulin et al.'s simulation – why does the initial open of the DP generate a vigorous MOC, and why does the simulated global MOC weaken with the deepening of the DP?

2 Methods

2.1 Model and simulations

The model configuration is based on an ocean-only sector model domain using the MIT general circulation model (MITgcm) (Marshall, Hill, et al., 1997; Marshall, Adcroft, et al., 1997). As shown in Figure 1, the model domain is composed of an ocean basin extending from 60°S to 60°N, and 0°E to 20°E. An ocean gateway is located in the latitudes of 60°S to 40°S. We refer to the ocean gateway as "OG" for the sake of convenience. The model domain has 1/6 ° horizontal grid spacing, allowing for mesoscale eddies. There are 42 unevenly spaced vertical levels with a 10 m thickness at the surface level, stretching to 250 m at the bottom, for a total depth of 5000 m. At the surface, temperature is restored to a fixed distribution, with a restoring time scale of 10 days. The sea surface temperature at the equator is restored to 30°C, the southern end of the domain to 0°C, and the northern end of the domain to 5°C. A linear equation of state is used for density with a constant salinity of 35 psu. There is no wind forcing or other mechanical forcing. The background vertical diffusivity is set to $K_v = 10^{-6}$ m^2s^{-1}. More details of the model configuration can be found in Klocker et al.(submitted).

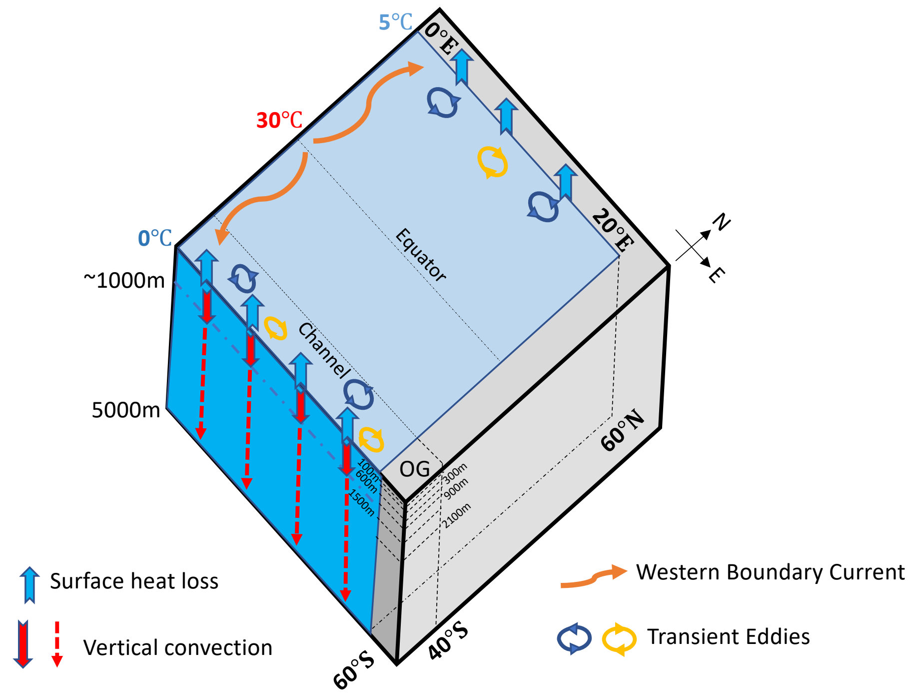

Figure 1. Schematic of model domain and ocean circulation. Orange curved arrows indicate western boundary current. In the channel (60°S - 40°S), colored circles are transient eddies, blue vertical arrows are surface heat loss. Solid (dashed) red vertical arrows at the southern end indicate convection in the cases of *OG_closed* (all experiments with an open OG).

An experiment with both a fully closed OG (*OG_closed*), and a fully open OG (*OG_open*), were run for 3000 model years in Klocker et al.(submitted). Based on these two existing cases, we conduct six sensitivity experiments in which we change the OG depths (the depth of the OG topography beneath sea surface) to 100 m (*OG_100*), 300 m (*OG_300*), 600 m (*OG_600*), 900 m (*OG_900*), 1500 m (*OG_1500*) and 2100 m (*OG_2100*). We run all six sensitivity experiments for 2500 model years from the *OG_closed* case, and use the final 50 years for our analysis.

2.2 Calculation of the meridional overturning circulation

To accurately describe the MOC, composed of horizontal and vertical flows along and across density surfaces, it is necessary to calculate the MOC in density coordinates

(Döös & Webb, 1994). We calculate the meridional transport (VH) between every density layer, where V is meridional velocity and H is thickness of density layer. We take the vertical integral of VH, then zonally integral and finally average over time to get the total MOC in density coordinates (Ballarotta et al., 2013), which can be written as:

$$\Psi^{\sigma}_{total} = \frac{1}{t_1 - t_0} \int_{t_0}^{t_1} \int_{x_W}^{x_E} \sum_{z^s_\sigma(\sigma)}^{z^b_\sigma(\sigma)} VH \, dx \, dt, \tag{1}$$

where x_W and x_E are the longitudes of the western and eastern boundaries of the model domain. z^s_σ and z^b_σ are surface and bottom density layer. t_0 and t_1 are the start and end point of the time average, respectively. Noting that the vertical sum is vertically accumulating density-binned VH.

We then use the thickness of density layers ($z_\sigma(\sigma)$) and the time-average density distribution in depth coordinates ($\sigma(x, y, z)$) to linearly interpolate the density-coordinate MOC into depth coordinates:

$$\Psi^{\sigma}_{total} \longrightarrow \Psi^{z}_{total}. \tag{2}$$

2.3 Calculation of meridional heat transport and vertical heat transport

The zonally integrated meridional heat transport (MHT) is calculated on each depth level as

$$MHT = \frac{\rho_0 C_\rho}{t_1 - t_0} \int_{t_0}^{t_1} \int_{x_W}^{x_E} VT \, dx, \tag{3}$$

where V is zonal velocity, T is potential temperature, ρ_0 is the reference density, and C_ρ is the specific heat capacity. When zonally and vertically integrating the meridional heat transport, we get

$$MHT_Z = \frac{\rho_0 C_\rho}{t_1 - t_0} \int_{t_0}^{t_1} \int_{x_W}^{x_E} \int_{z_b}^{z_s} VT \, dz \, dx \, dt, \tag{4}$$

where z^s and z^b are surface and bottom depth layer.

The vertical heat transport (VHT) is calculated by horizontally integrating the vertical advective flux of potential temperature at each depth level,

$$VHT = \frac{\rho_0 C_\rho}{t_1 - t_0} \int_{t_0}^{t_1} \int_A WT \, dA \, dt, \tag{5}$$

where W is the vertical velocity and A is horizontal area of the ocean domain.

2.4 Decomposition into eddy, standing-meander, and mean components

Using Reynolds averaging, an arbitrary field B can be decomposed into its time mean, $\overline{B}$, and transient eddy, B', components:

$$B = \overline{B} + B'. \tag{6}$$

Note that, by construction, $\overline{B'} = 0$.

The time mean component, $\overline{B}$, can be further separated into its zonal average part $\langle\overline{B}\rangle$ and the excursion from this average $\overline{B^*}$ (the so-called standing meanders component):

$$\overline{B} = \langle\overline{B}\rangle + \overline{B^*}. \tag{7}$$

The total field, B, is then given by:

$$B = \langle\overline{B}\rangle + \overline{B^*} + B'. \tag{8}$$

We can use Reynolds averaging to decompose the total transport of any tracer, such as temperature, into its mean, eddy, and standing meander components. The times and zonal averages operate on the product of meridional velocity and temperature in the equation (3). This produces three terms, since the covariance of $V^{'}$ and $T^{'}$ is not zero by construction. We can then decompose the total MHT_Z into three components:

$$MHT_Z = \rho_0 C_\rho \int_{x_W}^{x_E} \int_{z_b}^{z_s} \left[\langle \overline{V} \rangle \langle \overline{T} \rangle + \overline{V^* T^*} + \overline{V' T'} \right] dz\, dx, \tag{9}$$

where the first term of right side is mean flow component ($\langle \overline{MHT} \rangle_Z$), the second term is the standing meander component (MHT^*_Z), and the third term is transient eddy component ($MHT^{'}_Z$). Similarly, we use this decomposition for the vertical heat transport, giving $\langle \overline{VHT} \rangle$, VHT^* and $VHT^{'}$.

3 Results

3.1 Overturning circulation with fully open and fully closed gateway

Due to the heating of the ocean surface at the equator and cooling at high latitudes, ocean circulation adjusts to allow for a heat transport from the equator to high latitudes through a process known as (rotating) horizontal convection (G. O. Hughes & Griffiths, 2008; Gayen & Griffiths, 2022). In a closed basin, such as in experiment *OG_closed*, meridional boundaries allow for the generation of an east-west pressure gradient, and hence the poleward heat transport is due to western boundary currents (WBCs) associated with ocean gyres (Figure S1b). These WBCs transport heat poleward very efficiently and lead to a shallow MOC (Figure 2a), consistent with previous results (Klocker et al., submitted).

In the absence of meridional boundaries, such as in experiment *OG_open*, WBCs cannot exist in the latitude range of the channel (Figure S1j). At these latitudes only turbulent processes, such as mesoscale eddies, can transport heat across the channel (Figure 4i,j). These mesoscale eddies are generated by baroclinic instability due to steeply sloping density surfaces across the channel. These surfaces also generate a circumpolar current, resembling the Antarctic Circumpolar Current (Figure S1i), via thermal wind balance. As shown by Klocker et al. (submitted), the presence of eddies allows for a deep-reaching MOC, as opposed to the shallow MOC observed in the presence of meridional boundaries. In experiment *OG_open*, the surface buoyancy forcing generates a lower overturning cell with a strength (T_{MOC}) of 0.89 Sv, which is equivalent to 16.02 Sv when extrapolated from the width of the sector model to the full width of the ocean (Figure 2h,i).

For both *OG_closed* and *OG_open*, the MOC is closed by vertical plumes against the northern and southern headwall of the domain (G. Hughes et al., 2007; Gayen & Griffiths, 2022). In these regions, a destabilising buoyancy flux at the ocean surface leads to the formation of deep and bottom waters (Gayen & Griffiths, 2022). The heat in both cases can be transported by mean flows in the form of western boundary currents, or by mesoscale eddies across the re-entrant channel to generate an overturning cell. Below we will show that in the cases of partially open gateway there is a third process – standing meanders – which can lead to lateral and vertical heat transport, allowing for the formation of a deep-reaching MOC.

3.2 Deep-reaching overturning circulation with gateway deepening

A shallow OG, as in experiment *OG_100*, allows the formation of a vertically-sheared circumpolar current (Figure 2i). This circumpolar current is the result of the combination of buoyancy loss at the southern boundary, which, together with the lack of meridional boundaries above the OG depth, leads to the steepening of density surfaces and hence a (weak) associated circumpolar current with a zonal transport (T_{ACC}) of 3.1 Sv

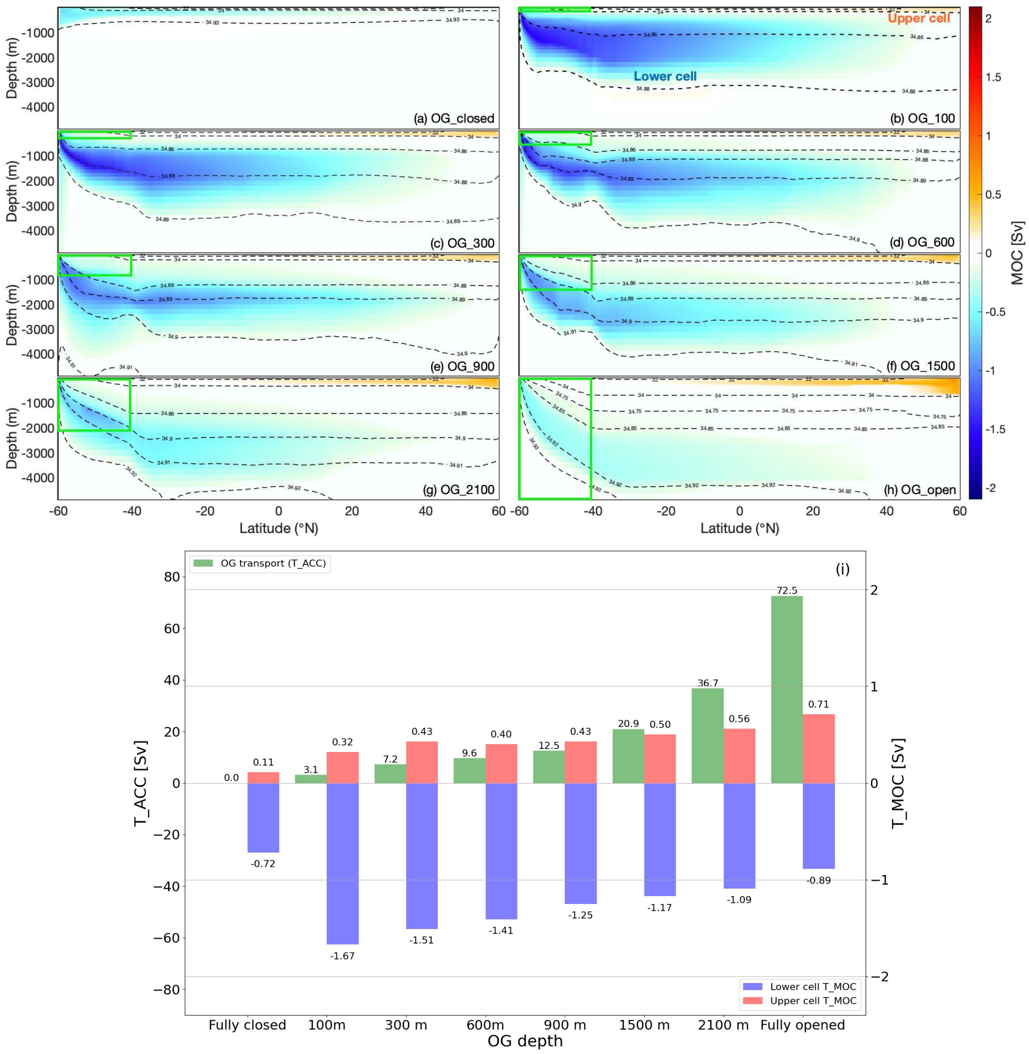

Figure 2. (a)-(h) MOC [Sv] of all simulations; clockwise cell (red) is the upper overturning cell and counterclockwise cell (blue) is the lower overturning cell. (i) Transport through OG ($T_{ACC}[Sv]$; green), maximum MOC ($T_{MOC}[Sv]$) for the upper cell (red) and the lower cell (blue).

(Figure 2i). This circumpolar current is baroclinically unstable, resulting in the generation of transient eddies and standing meanders, with the latter being generated due to the circumpolar current interacting with the topography of the OG.

A striking change is the deep-reaching MOC in *OG_100*; despite the very shallow OG, the lower overturning cell now extends to about 3500 m, and increases from 0.72 Sv in *OG_closed* to 1.67 Sv (global scale: 30.06 Sv; Figure 2b,i). This formation of a strong deep-reaching lower overturning cell is consistent with results by Klocker et al. (submitted), who showed how mesoscale eddies allow for a full-depth overturning cell, and with results by Toumoulin et al. (2020) who used a coarse-resolution earth system model with a 100 m deep DP and Eocene boundary conditions to simulate changes in the MOC due to gateway deepening.

With the deepening of the OG from 100 m to 2100 m (experiments *OG_100* to *OG_2100*), the transport of the eastward circumpolar current (T_{ACC}) gradually increases to 36.7 Sv (Figure 2i). In contrast with the increasing transport of the circumpolar current, the lower overturning cell continuously weakens to 1.09 Sv (global scale: 19.62 Sv) for the 2100 m OG experiment (Figure 2i). The shallowest OG therefore leads to the strongest lower overturning cell. This is consistent with recent results using a complex earth system model (Toumoulin et al., 2020).

3.3 The role of ocean heat transport

Buoyancy (heat) loss at the southern boundary of the channel leads to deep convection (Gayen & Griffiths, 2022) and hence the lower overturning cell. In an equilibrated ocean, maintaining the buoyancy loss and a deep-reaching overturning requires continuous lateral heat transport towards the southern ('Antarctic') boundary, and vertical heat transport to the deep ocean. The lower overturning cell is accordingly controlled by this heat transport. In this section, we will show how changes in OG depth affect the distribution of meridional and vertical heat transport by mean flows, standing meanders, and transient eddies.

For the experiment with a closed OG (*OG_closed*), the zonally integrated meridional heat transport is dominated by the mean flow (Figure 3a,b), transporting heat southward (blue colours) at the surface and northward (red colours) below. This is consistent with the MOC being confined to the shallow ocean, with the deep ocean being largely at rest (Figure 2a and Figure 3a-c). In the southern hemisphere, standing meanders produce a southward MHT (MHT^*) at the surface, and a northward MHT below. Transient eddies lead to a southward MHT across the channel, but contribute less to the heat transport than either the mean flow or standing meanders (Figure S4). The vertically integrated MHT (MHT_Z) is strongly biased towards the southern high latitudes, consistent with experiments of thermally-driven flows in a domain lacking a re-entrant channel, in which the flow is biased towards the pole with the colder temperature forcing (Coman et al., 2010, Figure 4a). Consistent with the shallow confinement of the MHT and MOC, the VHT is confined to the shallow ocean (Figure 4b). In summary, in *OG_closed* the entire heat transport is by baroclinic gyres which are confined to the ocean surface, leading to a shallow MOC. The deep ocean is at rest.

When the OG opens to a depth of 100 m (*OG_100*), the MHT suddenly extends to the full depth of the basin rather than being confined to the shallow ocean, with a southward MHT from surface to mid-depth, and a northward MHT below (Figure 3e). This corresponds to a full-depth lower overturning cell, which increases in strength from 0.72Sv to 1.67Sv. Standing meanders lead to a southward MHT above the OG depth, and a northward MHT below the OG depth (Figure 3f). Transient eddies still provide weak southward MHT in the channel. The total vertically and zonally integrated southward MHT (${MHT^*}_Z$) in the southern half of the basin is reduced by about half (maximum about -10 TW) compared to *OG_closed*, and is both due to the mean flow and standing me-

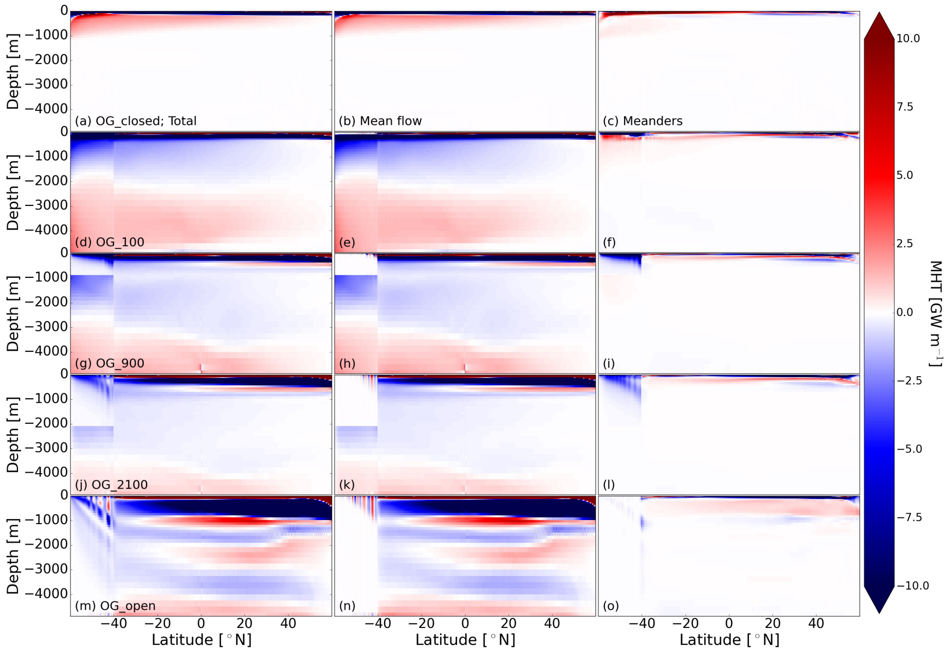

Figure 3. Hydrographic section of the zonally integrated meridional heat transport (MHT) [GW m^{-1}] for experiments *OG_closed*, *OG_100*, *OG_900*, *OG_2100*, and *OG_open*. Left panels show total MHT, middle panels show the MHT by the mean flow ($\langle\overline{MHT}\rangle$), and right panels show the MHT by standing meanders (MHT^{*}).

anders (Figure 4c). On the other hand, the northward MHT in the northern half of the basin increases by 8 TW compared to *OG_closed*. Transient eddies again provide little MHT (MHT'_Z) relative to the mean flow and standing meanders. In contrast to the large decrease in MHT by the mean flow in *OG_100*, the VHT by the mean flow shows a large increase in strength and now extends to the full depth (Figure 4d).

For a further OG deepening (from *OG_100* to *OG_2100*), the mean MHT in the deep ocean decreases in strength compared with *OG_100*, reflected by lighter blue and red colors in the Figure 3h and k. This corresponds to a weakening of the deep-reaching MOC. In the channel, standing meanders lead to a southward MHT above the OG depth. The MHT by transient eddies increases, although it is still weaker than the other terms. The gradual deepening of the OG strengthens the transport of the circumpolar current, and leads to a state where the vertically integrated MHT is entirely due to standing meanders (Figure 4e and g) in the channel. The MHT by standing meanders becomes weaker the deeper the OG, leading to a decrease in strength of the lower overturning cell for a further OG deepening. This weakening of the southward MHT is accompanied by a strengthening of the northward MHT, and hence a stronger upper overturning cell.

When the OG is fully open (*OG_open*), standing meanders cannot exist since their existence relies on the interaction with a ridge, and instead transient eddies provide southward MHT. For this experiment the MOC is still full-depth, but weaker than in all cases where standing meanders are present. This experiment therefore shows that eddies are also capable of allowing for a full-depth lower overturning cell, but given that transient eddies are less efficient at transporting heat towards the southern convection region, the lower overturning cell is weaker than in all cases where standing meanders are present.

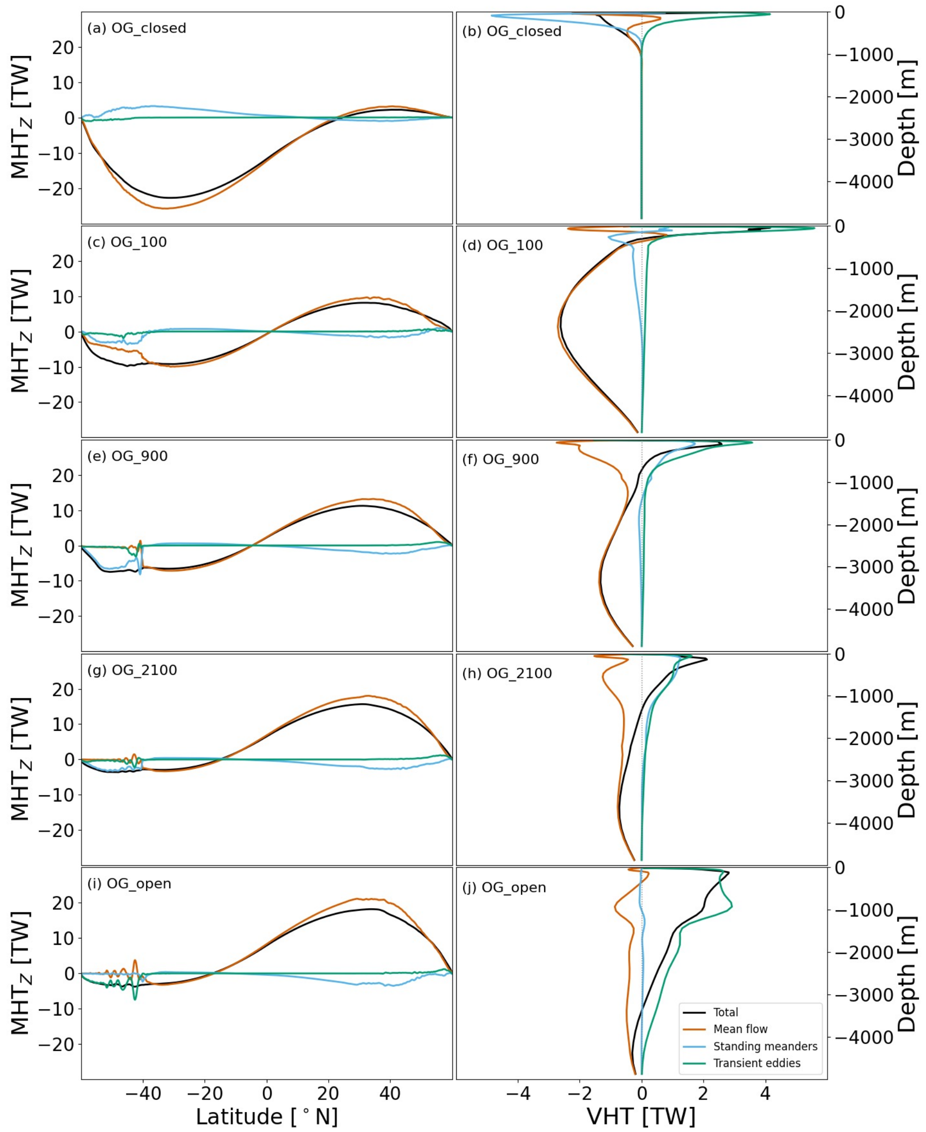

Figure 4. (a,c,e,g,i) Zonally and vertically integrated meridional heat transport (MHT_Z) [TW] for experiments *OG_closed*, *OG_100*, *OG_900* , *OG_2100*, and *OG_open*. (b,d,f,h,j) Horizontal integrated vertical heat transport (VHT) [TW] in the channel for experiments *OG_closed*, *OG_100*, *OG_900*, *OG_2100*, and *OG_open*. In all panels, black lines indicate the total (MHT_Z/VHT), red lines the mean component ($\langle\overline{MHT}\rangle_Z/\langle\overline{VHT}\rangle$), green lines the standing meanders ($MHT^{*}{}_Z/VHT^{*}$), and blue lines the transient eddies ($MHT^{'}{}_Z/VHT^{'}$).

4 Discussion and Conclusion

In summary, the evolution of the deep-reaching lower overturning cell with the deepening of the ocean gateway can be divided into two parts: the abrupt onset of the deep-reaching lower overturning cell for a shallow ocean gateway, and the subsequent weakening for a further deepening of the ocean gateway. This behaviour of the lower overturning cell is closely linked to changes in southward and downward heat transport in the presence of standing meanders. First, in an equilibrated ocean, the strength of an overturning cell is limited by the amount of heat which can be supplied to the vertical plumes associated with strong surface buoyancy loss. This heat supply is most efficient if mean flows, such as western boundary currents, are present. This heat supply becomes less efficient if the heat transport is due to standing meanders, and even less efficient if heat supply is due to transient eddies. A deepening ocean gateway therefore leads to a reduced southward heat transport, which is compensated with an increase in northward heat transport. Second, a deep-reaching overturning cell is dependent on a process which can get this heat to depth. As shown by Klocker et al. (submitted), this can be achieved by transient eddies, and, as shown here, this can also be achieved by standing meanders. Nevertheless, heat transport by baroclinic gyres is always confined to the surface, and the presence of mesoscale turbulence, whether transient eddies or standing meanders, is necessary to get this heat to depth, and hence lead to a deep-reaching MOC.

The two-part evolution of the lower overturning cell for a deepening of an ocean gateway is therefore a combination of the two roles transient eddies and standing meanders play for ocean heat transport. These dynamics lead to a maximum lower overturning cell for the experiment with the shallowest OG, which is a combination of the domain where the southward heat transport is largest, while at the same time allowing for a deep-reaching heat transport by mesoscale turbulence. Further deepening of the OG leads to a weakening of the southward heat supply across the channel, and a strengthening of the northward heat transport, associated with a strengthening of the upper overturning cell. Once the OG is as deep as the rest of the domain, the southward heat transport is solely due to transient eddies, resulting in the weakest deep-reaching overturning cell. As opposed to studies which focus on just fully open and fully closed OGs, we highlight the importance of the dynamics of standing meanders in understanding the evolution of the MOC with gateway deepening, a turbulent process generally neglected in the paleoceanography community.

Previous studies have used complex, but coarse-resolution, earth system models to explain the evolution of the global MOC with the deepening of Southern Ocean gateways (Sijp & England, 2004; Toumoulin et al., 2020). However, in these studies results contradict each other, with (Sijp & England, 2004) showing the strongest MOC for a closed OG, while (Toumoulin et al., 2020), consistent with our study, showing the strongest MOC for a shallow OG. Nevertheless, both these studies show a weakening of the southward meridional heat transport with a deepening of the OG, and a strengthening of the northward meridional heat transport, consistent with our study. The different results for the lower overturning cell are possibly the consequence of the parameterisation of mesoscale turbulence in these models. It is the simple but high-resolution model configuration used in this study that helps to reveal the critical role of turbulence processes in generating the strong deep-reaching overturning cell with OG deepening. Future work is planned to extend this work on the evolution of the EOT MOC with a global ocean model and realistic paleo-bathymetry.

5 Data Availability Statement

All model output used in this study to perform the analysis and produce figures is available at https://doi.org/10.5281/zenodo.7602996.

Acknowledgments

This work was supported by the Australian Research Council Discovery Project (DP180102280). QX was supported by scholarships from the Australian Government Research Training Program (RTP) and CSIRO-UTAS PhD Program in Quantitative Marine Science (QMS). We acknowledge the Australian National Computational Infrastructure Merit Allocation Scheme projects and Australian Antarctic Division grant AAS4567 for running the model simulations.

References

Abelson, M., & Erez, J. (2017). The onset of modern-like a tlantic meridional overturning circulation at the e ocene-o ligocene transition: Evidence, causes, and possible implications for global cooling. *Geochemistry, Geophysics, Geosystems*, *18*(6), 2177–2199.

Ballarotta, M., Drijfhout, S., Kuhlbrodt, T., & Döös, K. (2013). The residual circulation of the southern ocean: Which spatio-temporal scales are needed? *Ocean Modelling*, *64*, 46–55.

Borrelli, C., Cramer, B. S., & Katz, M. E. (2014). Bipolar atlantic deepwater circulation in the middle-late eocene: Effects of southern ocean gateway openings. *Paleoceanography*, *29*(4), 308–327.

Boyle, P. R., Romans, B. W., Tucholke, B. E., Norris, R. D., Swift, S. A., & Sexton, P. F. (2017). Cenozoic north atlantic deep circulation history recorded in contourite drifts, offshore newfoundland, canada. *Marine Geology*, *385*, 185–203.

Cessi, P. (2019). The global overturning circulation. *Annual review of marine science*, *11*, 249–270.

Coman, M., Griffiths, R., & Hughes, G. (2010). The sensitivity of convection from a horizontal boundary to the distribution of heating. *Journal of Fluid Mechanics*, *647*, 71–90.

Döös, K., & Webb, D. J. (1994). The deacon cell and the other meridional cells of the southern ocean. *Journal of Physical Oceanography*, *24*(2), 429–442.

Ferreira, D., Cessi, P., Coxall, H. K., De Boer, A., Dijkstra, H. A., Drijfhout, S. S., ... others (2018). Atlantic-pacific asymmetry in deep water formation. *Annual Review of Earth and Planetary Sciences*, *46*, 327–352.

Foppert, A., Donohue, K. A., Watts, D. R., & Tracey, K. L. (2017). Eddy heat flux across the a ntarctic c ircumpolar c urrent estimated from sea surface height standard deviation. *Journal of Geophysical Research: Oceans*, *122*(8), 6947–6964.

Gayen, B., & Griffiths, R. W. (2022). Rotating horizontal convection. *Annual Review of Fluid Mechanics*, *54*, 105–132.

Hague, A. M., Thomas, D. J., Huber, M., Korty, R., Woodard, S. C., & Jones, L. B. (2012). Convection of north pacific deep water during the early cenozoic. *Geology*, *40*(6), 527–530.

Hohbein, M. W., Sexton, P. F., & Cartwright, J. A. (2012). Onset of north atlantic deep water production coincident with inception of the cenozoic global cooling trend. *Geology*, *40*(3), 255–258.

Hughes, C. W. (2005). Nonlinear vorticity balance of the antarctic circumpolar current. *Journal of Geophysical Research: Oceans*, *110*(C11).

Hughes, G., Griffiths, R., Mullarney, J., & Peterson, W. H. (2007). A theoretical model for horizontal convection at high rayleigh number. *Journal of Fluid Mechanics*, *581*, 251–276.

Hughes, G. O., & Griffiths, R. W. (2008). Horizontal convection. *Annu. Rev. Fluid Mech.*, *40*, 185–208.

Hutchinson, D. K., Coxall, H. K., Lunt, D. J., Steinthorsdottir, M., De Boer, A. M., Baatsen, M., ... others (2021). The eocene–oligocene transition: a review of marine and terrestrial proxy data, models and model–data comparisons. *Climate of the Past*, *17*(1), 269–315.

Ivchenko, V. O., Richards, K. J., & Stevens, D. P. (1996). The dynamics of the antarctic circumpolar current. *Journal of physical oceanography*, *26*(5), 753–774.

Johnson, G. C. (2008). Quantifying antarctic bottom water and north atlantic deep water volumes. *Journal of Geophysical Research: Oceans*, *113*(C5).

Johnson, H. L., Cessi, P., Marshall, D. P., Schloesser, F., & Spall, M. A. (2019). Recent contributions of theory to our understanding of the atlantic meridional overturning circulation. *Journal of Geophysical Research: Oceans*, *124*(8), 5376–5399.

Katz, M. E., Cramer, B. S., Toggweiler, J., Esmay, G., Liu, C., Miller, K. G., ... Wright, J. D. (2011). Impact of antarctic circumpolar current development on late paleogene ocean structure. *Science*, *332*(6033), 1076–1079.

Klocker, A., Munday, D., Gayen, B., Roquet, F., & LaCasce, J. H. (submitted). Deep-reaching global ocean overturning circulation generated by surface buoyancy forcing. *Journal of Physical Oceanography*.

Kuhlbrodt, T., Griesel, A., Montoya, M., Levermann, A., Hofmann, M., & Rahmstorf, S. (2007). On the driving processes of the atlantic meridional overturning circulation [Journal Article]. *Reviews of Geophysics*, *45*(2).

Marshall, J., Adcroft, A., Hill, C., Perelman, L., & Heisey, C. (1997). A finite-volume, incompressible navier stokes model for studies of the ocean on parallel computers. *Journal of Geophysical Research: Oceans*, *102*(C3), 5753–5766.

Marshall, J., Hill, C., Perelman, L., & Adcroft, A. (1997). Hydrostatic, quasi-hydrostatic, and nonhydrostatic ocean modeling. *Journal of Geophysical Research: Oceans*, *102*(C3), 5733–5752.

Marshall, J., & Speer, K. (2012). Closure of the meridional overturning circulation through southern ocean upwelling. *Nature Geoscience*, *5*(3), 171–180.

Sijp, W. P., & England, M. H. (2004). Effect of the drake passage throughflow on global climate. *Journal of Physical Oceanography*, *34*(5), 1254–1266.

Talley, L. D. (2013). Closure of the global overturning circulation through the indian, pacific, and southern oceans: Schematics and transports. *Oceanography*, *26*(1), 80–97.

Thomas, D. J. (2004). Evidence for deep-water production in the north pacific ocean during the early cenozoic warm interval. *Nature*, *430*(6995), 65–68.

Thomas, D. J., Korty, R., Huber, M., Schubert, J. A., & Haines, B. (2014). Nd isotopic structure of the pacific ocean 70–30 ma and numerical evidence for vigorous ocean circulation and ocean heat transport in a greenhouse world. *Paleoceanography*, *29*(5), 454–469.

Toggweiler, J., & Bjornsson, H. (2000). Drake passage and palaeoclimate. *Journal of Quaternary Science: Published for the Quaternary Research Association*, *15*(4), 319–328.

Toumoulin, A., Donnadieu, Y., Ladant, J.-B., Batenburg, S., Poblete, F., & Dupont-Nivet, G. (2020). Quantifying the effect of the drake passage opening on the eocene ocean. *Paleoceanography and Paleoclimatology*, *35*(8), e2020PA003889.

Youngs, M. K., Thompson, A. F., Lazar, A., & Richards, K. J. (2017). Acc meanders, energy transfer, and mixed barotropic–baroclinic instability. *Journal of Physical Oceanography*, *47*(6), 1291–1305.

Zhang, X., Nikurashin, M., Peña-Molino, B., Rintoul, S. R., & Doddridge, E. (2023). A theory of standing meanders of the antarctic circumpolar current and their response to wind. *Journal of Physical Oceanography*, *53*(1), 235 - 251. doi: 10.1175/JPO-D-22-0086.1

Supporting Information for Deepening of Southern Ocean gateway leads to abrupt onset of vigorous meridional overturning circulation

Qianjiang Xing[1], Andreas Klocker[2], David Munday[3], Joanne Whittaker[1]

[1]Institute for Marine and Antarctic Studies, University of Tasmania, Hobart, Australia

[2]NORCE Norwegian Research Centre, Bjerknes Centre for Climate Research, Bergen, Norway

[3]British Antarctic Survey, Cambridge, United Kingdom

Contents of this file

Figures S1 to S5

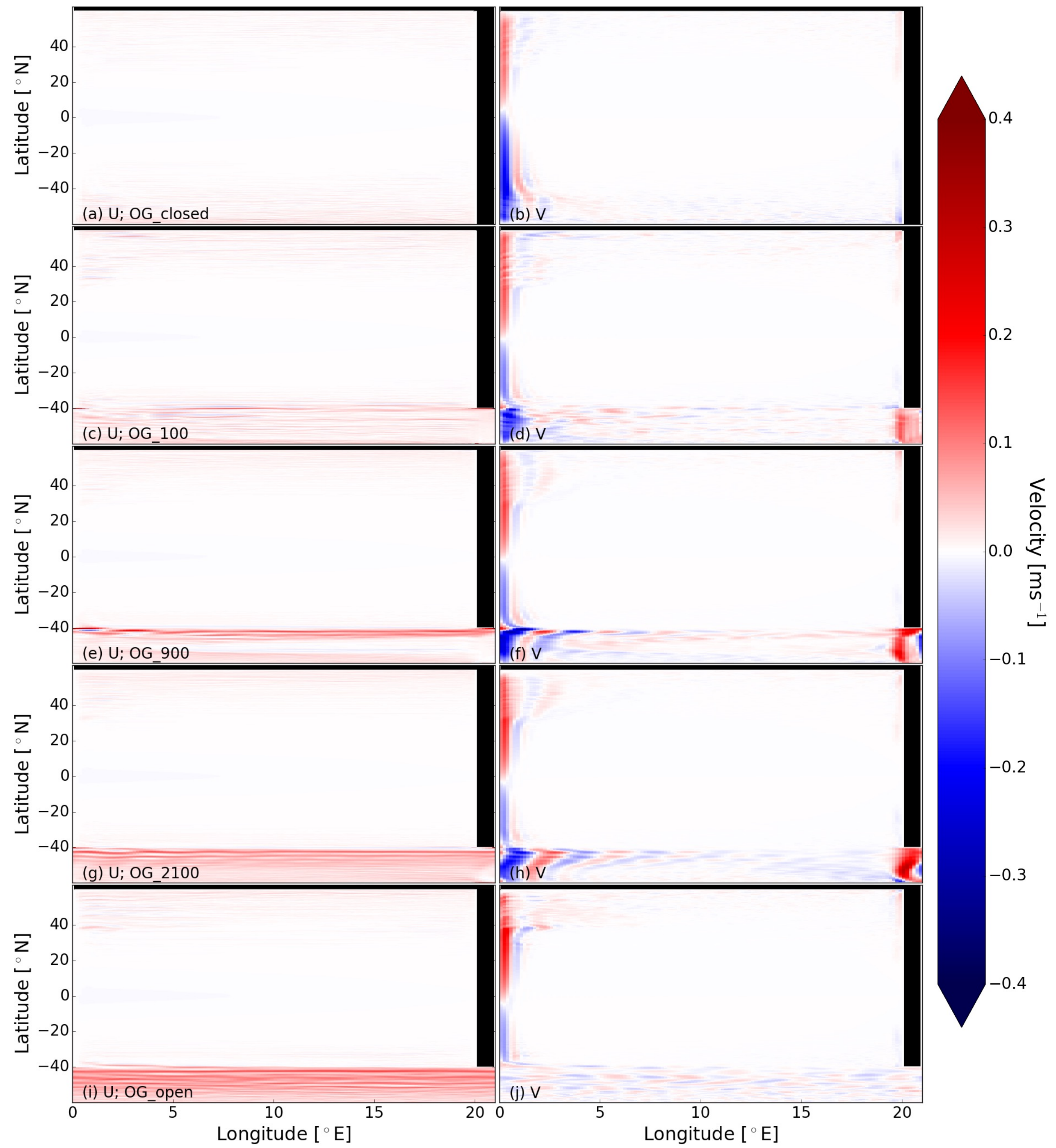

Figure S1. (a,c,e,g) Sea surface zonal velocity [m s^{-1}], (b,d,f,h) Sea surface meridional velocity [m s^{-1}] for *OG_closed*, *OG_100*, *OG_900*, *OG_2100*, and *OG_open*.

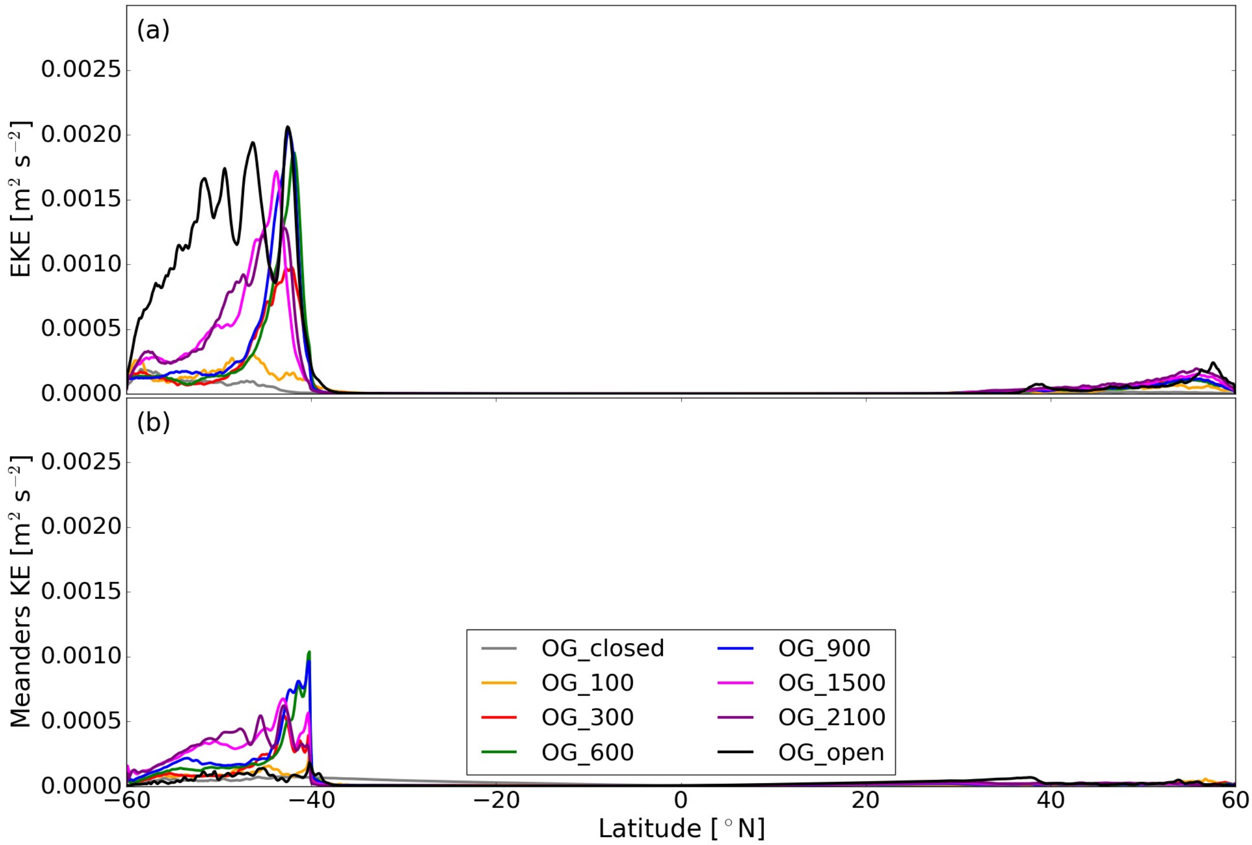

Figure S2. (a) Zonally and vertically mean kinetic energy of transient eddies; (b) Zonally and vertically mean kinetic energy of standing meanders. Colored lines show different simulations: *OG_closed* (grey), *OG_100* (orange), *OG_300* (red), *OG_600* (green), *OG_900* (blue), *OG_1500* (magenta), *OG_2100* (purple), and *OG_open* (black).

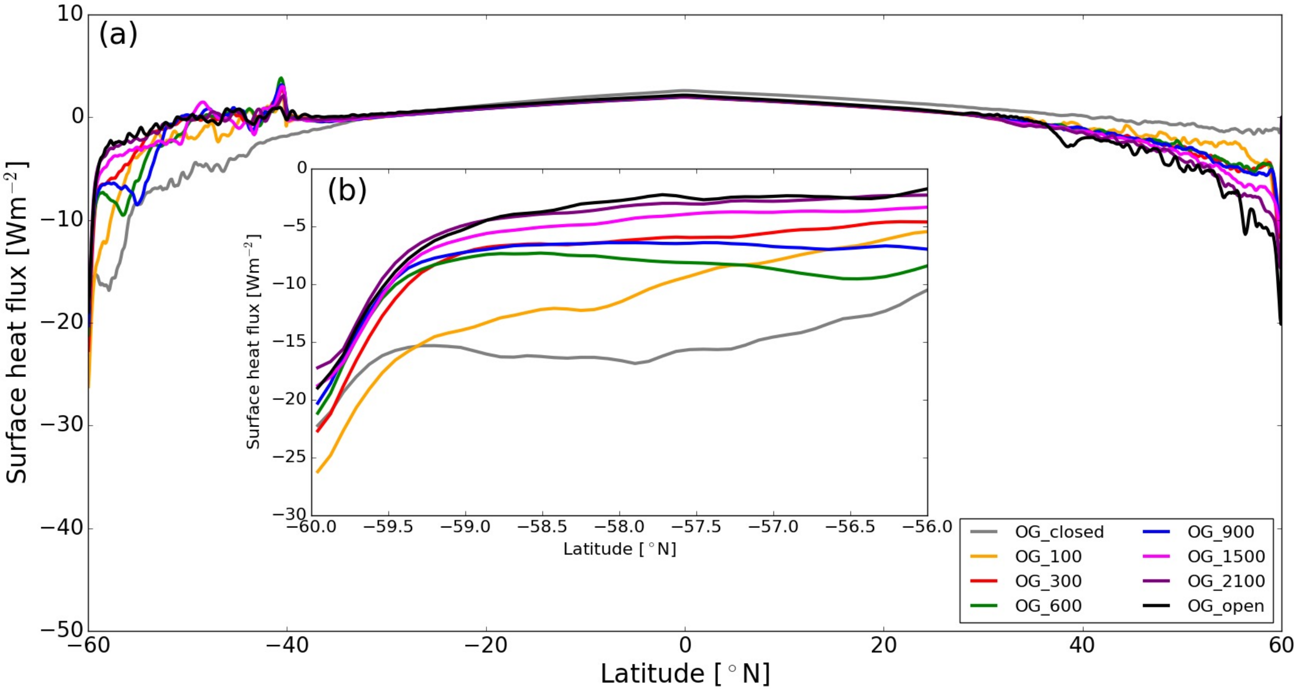

Figure S3. Zonally mean surface heat flux [W m^{-2}] for (a) the full domain, and (b) zoomed in on the south of the domain. Colored lines show different simulations: *OG_closed* (grey), *OG_100* (orange), *OG_300* (red), *OG_600* (green), *OG_900* (blue), *OG_1500* (magenta), *OG_2100* (purple), and *OG_open* (black).

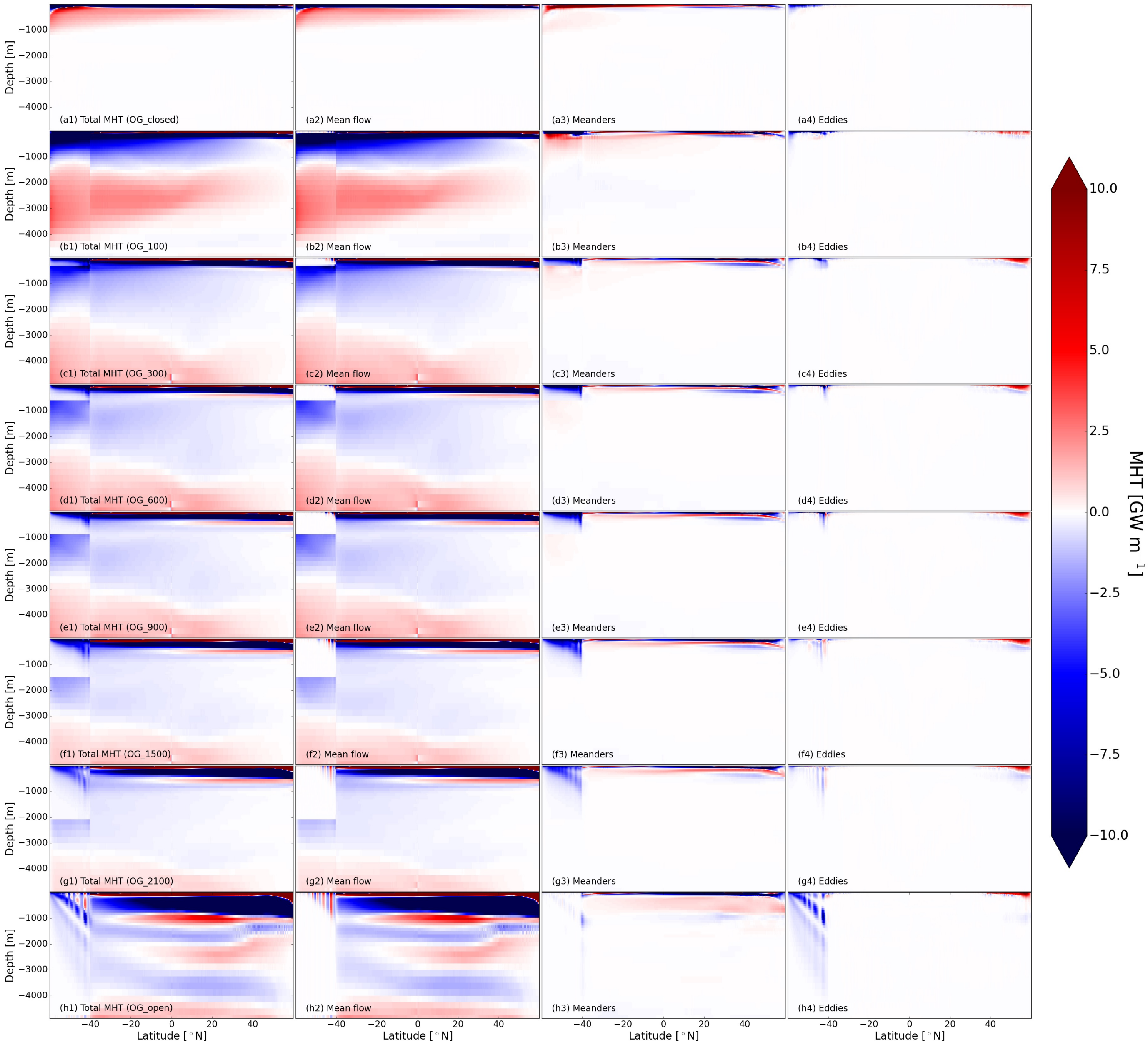

Figure S4. Hydrographic sections of zonally integrated meridional heat transport (MHT) [10^{-2} TW m^{-1}] for *OG_closed*, *OG_100*, *OG_300*, *OG_600*, *OG_900*, *OG_1500*, *OG_2100*, and *OG_open*. (a1, b1, c1, d1, e1, f1, g1, h1) total MHT, (a2, b2, c2, d2, e2, f2, g2, h2) mean flow $\langle\overline{MHT}\rangle$, (a3, b3, c3, d3, e3, f3, g3, h3) meanders MHT^{*}, (a4, b4, c4, d4, e4, f4, g4, h4) eddy $MHT^{'}$.

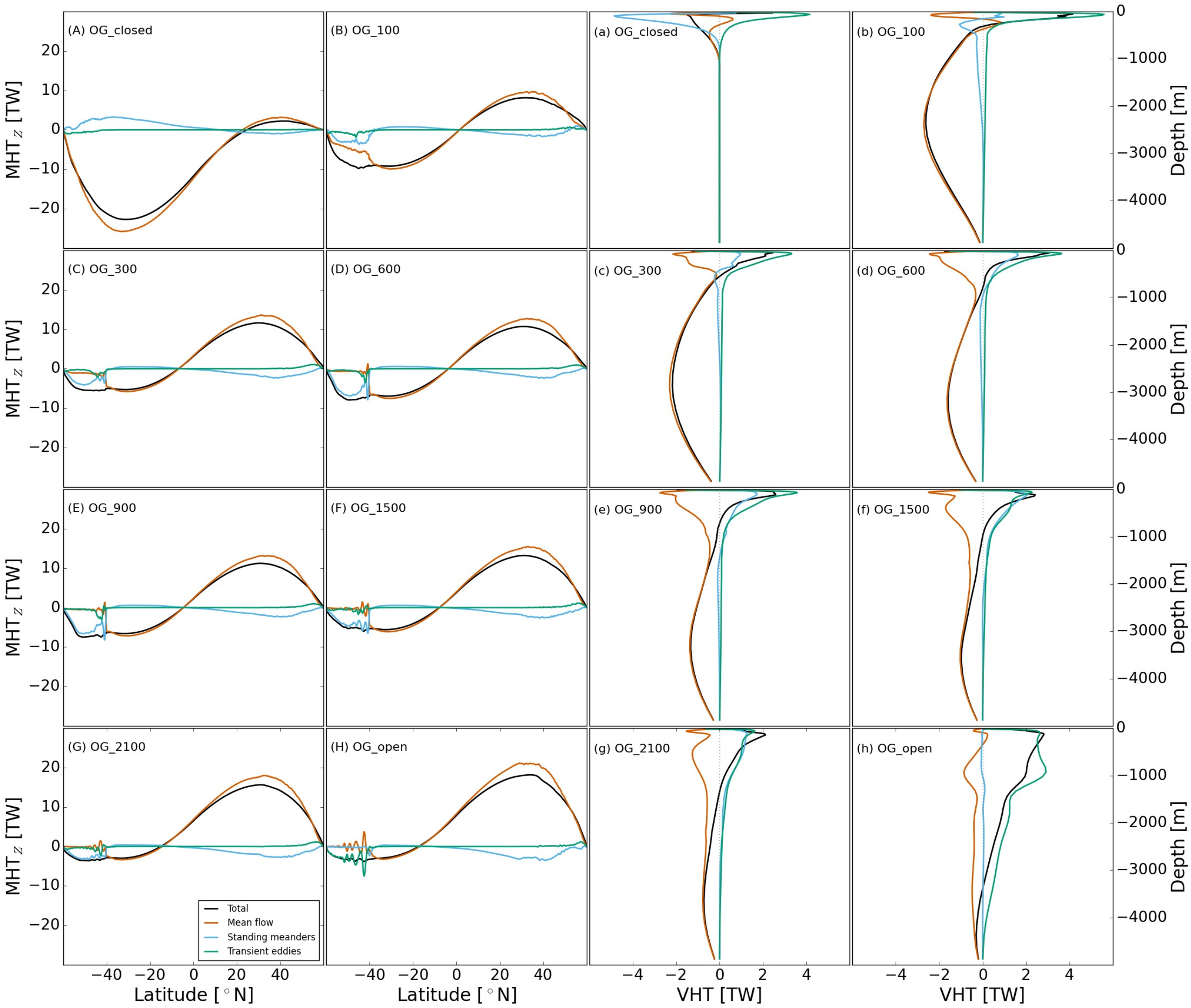

Figure S5. (A-H) Zonally and vertically integrated meridional heat transport (MHT_z) [TW]; (a-h) Horizontal mean vertical heat transport (VHT) [TW] in the channel for *OG_closed*, *OG_100*, *OG_300*, *OG_600*, *OG_900*, *OG_1500*, *OG_2100*, and *OG_open*. Black lines show total MHT_z/VHT, red lines indicate the mean flow $\langle\overline{MHT}\rangle_z/\langle\overline{VHT}\rangle$, green lines describe standing meanders $MHT^*{}_z/VHT^*$, and blue lines show transient eddy $MHT'{}_z/VHT'$.